ACS OMEGA

Open Access

This article is licensed under CC-BY-NC-ND 4.0

http://pubs.acs.org/journal/acsodf

Article

Performance Evaluation of Benzyl Alcohol Oxidation with *tert*-Butyl Hydroperoxide to Benzaldehyde Using the Response Surface Methodology, Artificial Neural Network, and Adaptive Neuro-Fuzzy Inference System Model

Ikenna Chibuzor Emeji,* Michael Kumi, and Reinout Meijboom

Cite This: *ACS Omega* 2024, 9, 34464−34481

Read Online

ACCESS | Metrics & More | Article Recommendations | Supporting Information

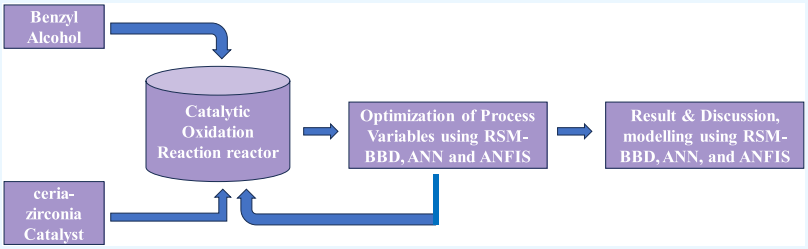

ABSTRACT: The adaptive neuro-fuzzy inference system (ANFIS), central composite experimental design (CCD)-response surface methodology (RSM), and artificial neural network (ANN) are used to model the oxidation of benzyl alcohol using the *tert*-butyl hydroperoxide (TBHP) oxidant to selectively yield benzaldehyde over a mesoporous ceria-zirconia catalyst. Characterization reveals that the produced catalyst has hysteresis loops, a sponge-like structure, and structurally induced reactivity. Three independent variables were taken into consideration while analyzing the ANN, RSM, and ANFIS models: the amount of catalyst (A), reaction temperature (B), and reaction time (C). With the application of optimum conditions, along with a constant (45 mmol) TBHP oxidant amount, (30 mmol) benzyl alcohol amount, and rigorous refluxing of 450 rpm, a maximum optimal benzaldehyde yield of 98.4% was obtained. To examine the acceptability of the models, further sensitivity studies including statistical error functions, analysis of variance (ANOVA) results, and the lack-of-fit test, among others, were employed. The obtained results show that the ANFIS model is the most suited to predicting benzaldehyde yield, followed by RSM. Green chemistry matrix calculations for the reaction reveal lower values of the *E*-factor (1.57), mass intensity (MI, 2.57), and mass productivity (MP, 38%), which are highly desirable for green and sustainable reactions. Therefore, utilizing a ceria-zirconia catalyst synthesized via the inverse micelle method for the oxidation of benzyl alcohol provides a green and sustainable methodology for the synthesis of benzaldehyde under mild conditions.

1. INTRODUCTION

Selective oxidation of benzyl alcohol to benzaldehyde is a significant process, and the product benzaldehyde has an enormous value as a raw material for a large number of products.[1−5] Benzaldehyde is the simplest aromatic aldehyde, extensively used in both industrial and consumer applications. These include pharmaceuticals, agrochemicals, chemical synthesis, flavor and fragrance, preservatives, and perfumery.[6−9] In addition, the oxidation of benzyl alcohol is frequently used as a model process for the oxidation of alcohols.[10] Although homogeneous catalysts are frequently used, they have several drawbacks, including corrosiveness, the ability to create undesirable byproducts, being difficult to separate from the reaction mixture, and nonreusability.[11−13] Consequently, clean and highly effective heterogeneous solid catalysts have been proposed recently, with a wide range of methods, which are more environmentally and economically friendly. Most of the proposed alternatives tend to combine the solid catalysts in solvent-free procedures (to minimize solvents), under mild circumstances (to conserve energy), with strong oxidants that are inexpensive and safe.[14,15] However, greater efforts are directed toward identifying green chemistry metrics to evaluate the sustainability and environmental impact of the benzyl alcohol oxidation reaction. As a result, parameters like the *E*-factor, mass intensity (MI), and mass productivity were used to gauge the greenness of the reaction or any process.[16−19] With waste being defined as "everything (except water) but the

Received: March 8, 2024
Revised: June 5, 2024
Accepted: June 11, 2024
Published: July 29, 2024

© 2024 The Authors. Published by American Chemical Society

desired product", the *E*-factor (eq 1) is the actual quantity of waste produced for a given mass of product generated.[16,20] Therefore, a higher *E*-factor value is an indication of more waste and, consequently, greater negative environmental impact. The ideal *E*-factor is zero, conforming to the first principle of green chemistry: "It is better to prevent waste than to treat or clean up waste after it is formed".[17,21] Conversely, zero waste and more sustainable and environmentally friendly processes are indicated by *E*-factor values that are closer to 0. Thus, lower *E*-factors are positively correlated with cheaper production costs, lower disposal costs for hazardous and toxic waste, higher capacity utilization, and lower energy consumption.[17,21] Additionally, the *E*-factor range for solvent-free reactions that just considered the synthesis phase was 0.1−4.0, placing them in the waste production group for bulk compounds.[22] However, all of the reactants, that is, reagents, solvents, catalysts, and any additional materials involved in the reaction, are included in mass productivity (MP, eq 2). MP represents the percentage of the intended product's mass relative to the overall mass of the reactants. An alternative definition of it would be the reciprocal expressed as a percentage of the mass intensity (MI). Mass intensity (MI), which is defined as the mass of all components added, except water, to the mass of the finished product, is connected to the *E*-factor by way of eq 3[19,23]

$$E\text{-Factor} = \frac{\text{Total mass of waste}}{\text{mass of desired product}} \quad (1)$$

$$\text{MP}\ (\%) = \frac{\text{mass of desired product} \times 100}{\text{total mass of used materials}} = \frac{1}{\text{MI}} \times 100 \quad (2)$$

$$\text{MI} = E\text{-Factor} + 1 \quad (3)$$

Mesoporous materials, in recent times, have seen a dramatic increase in their application as a catalyst because of their tenable structural characteristics, including surface area, nanocrystalline walls, pore volume, and size. Mesostructured ceria have drawn a lot of attention as heterogeneous catalysts due to their excellent oxygen storage capacity (OSC) and redox capabilities.[24] The excellent catalytic activity of ceria for all oxidation reactions was attributed to their high redox property (Ce^{3+} // Ce^{4+}) and oxygen lability in the lattice structure.[25] Among several other roles, cerium is utilized in catalysis involving the dehydrogenation of alcohols.[26] Recent rising interest in sciences has found that doping can also improve the catalytic activity of a catalyst. Jin et al.[27] showed that metal oxides doped on certain catalytic materials exhibited improved catalytic activity. Significant studies have been conducted on mesoporous transition-metal oxide materials, which include group I−IV elements Nb, Ta, Y, Ti, Mo, W, Cr, Zr, V, and Hf.[28,29] Therefore, incorporating Zr^{4+} into ceria's catalyst crystalline lattice impacts the Ce^{3+} // Ce^{4+} redox property and their oxygen storage capacity (OSC).[30,31] To achieve homogeneity and increase the OSC of the catalyst, an appropriate preparation method is necessary. In this study, the inverse surfactant micelle sol−gel method was used to prepare ceria-zirconia (CeO_2−ZrO_2) of different catalyst loadings. The surfactant species used is (poly(ethylene glycol)-*block*-poly-(propylene glycol)-*block*-poly(ethylene glycol)) (P-123). This method has several advantages: high selectivity, high mass and activity recovery, elimination of solvent effects, simple operation, cost-effectiveness, minimizing the effect of water content, and usage of nontoxic substances.[32] In another development, technical advancements in the Fourth Industrial Revolution have significantly led to drastic industrial changes. These changes have innovatively incorporated computational strategies into chemical reactions, thereby encouraging a more effective and productive output and hence revealing an in-depth ability to understand a fluid's relationship in reactors. Previous studies on the oxidation process, involving the conversion of benzyl alcohol to benzaldehyde (Figure 1, modified from Pérez et al.[33]), have concentrated on the one factor at a time (OFAT) method using traditional methods.

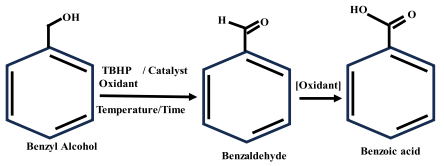

Figure 1. Oxidation process for converting benzyl alcohol to benzaldehyde.

In addition to taking a lot of time, OFAT is unable to forecast the intended optimum yield based on how the process variables interact. Instead, new computational methods like machine learning can help scientists save time and money by testing thousands of conditions in a short space of time for a better understanding of the complexity of chemical reactions. The machine-learning methods reveal the relationship between input variables and their interactive effects to predict an output.[34] Numerous studies have been reported on the successful applicability of response surface methodology (RSM), artificial neural network (ANN), and adaptive neuro-fuzzy inference system (ANFIS)-based modeling in predicting yields in chemical reactions. Rekhate and Shrivastava[35] applied RSM and ANN in forecasting the oxidation of acidic black azo dye using O_3, O_3/UV, and O_3/Fe(II) oxidation processes. With the aid of a UV−vis spectrophotometer, the decolorization process was ascertained in their investigation by measuring the dye's absorption wavelength. The potential consequences of the O_3, O_3/UV, and O_3/Fe(II) processes were accurately anticipated by the RSM and ANN modeling methods. In a statistical comparison, the group discovered that the ANN forecasts were superior to those of RSM. Additionally, Onu et al.[36] successfully modeled the anaerobic digestion process for biogas production using ANFIS, ANN, and RSM models. Also, in a comparative study on photovoltaic power, Jazayeri et al.[37] used ANN modeling with the application of Levenberg−Marquardt (LM) and Bayesian regularization (BR) training methods. The power output (W) and irradiation levels (W/m^2) of the solar cells were used to evaluate performance abilities. Longer training times were mitigated by BR's superior performance compared to LR.

The robust nature of these models made their usage necessary. The utilization of RSM is based on its capacity to minimize the number of experimental runs needed to assess the impact of various variables and their combined effects on the response. It has been widely used in a variety of chemical processes, including the production of biodiesel and biogas. ANN, on the other hand, has the capability to model and simulate nonlinear and extremely complicated systems due to its ability to employ learning algorithms to determine the relationship between input and output variables. Furthermore, ANFIS is regarded as a combination of neural networks and

https://doi.org/10.1021/acsomega.4c02174
ACS Omega 2024, 9, 34464−34481

fuzzy systems and therefore possesses the synergistic benefits of both techniques. From the literature review, no scientific investigation has previously been published dealing with the application of advanced modeling techniques like response surface methodology (RSM), artificial neural network (ANN), and adaptive neuro-fuzzy inference system (ANFIS) as indicated in the graphical abstract to the oxidation process for the conversion of benzyl alcohol to benzaldehyde. This study is therefore the first of its kind focusing on using advanced modeling techniques to simulate benzyl alcohol oxidation to benzaldehyde. Hence, possible model limitations encountered include model overfitting, the curse of dimensionality, interpretability problems with larger inputs, and difficulty selecting the appropriate membership functions. Such limitations were minimized with effective training protocols, appropriate input parameters, minimum error between the experimental and predicted values of the applicable models, and good prediction accuracy.[38,39] Thus, the primary goals of this research are (i) to prepare and characterize the ceria-zirconium catalyst using a novel inverse micelle method; (ii) to model the percentage yield of benzaldehyde conversion using machine-learning algorithms such as RSM, ANN, and ANFIS; and (iii) to critically verify, with full insight, the prediction capabilities of the three models using statistical analysis.

2. EXPERIMENTAL SECTION

2.1. Materials. All chemicals purchased were of reagent grade and were used as received. Cerium(III) nitrate hexahydrate [$Ce(NO_3)_3{\cdot}6H_2O$], zirconium(IV) butoxide [$Zr(OC_4H_9)_4$], Pluronic P-123, *tert*-butyl hydroperoxide (TBHP) (70% in water), and decane (99%) were bought from Sigma-Aldrich. Rochelle Chemicals (South Africa) provided 70% concentrated nitric acid (HNO_3).

2.2. Method for the Preparation of Mesoporous Cerium Oxide (Ceria). The procedural preparation of CeO_2 was derived from the existing literature[32,40] P-123 surfactant (5 g, 8.2×10^{-4} mol) was mixed in 1-butanol (56 g, 0.75 mol) and HNO_3 (8 g, 0.128 mol), which is contained in a 150 mL beaker. Cerium(III) nitrate hexahydrate salt ($Ce(NO_3)_3{\cdot}6H_2O$) (10 g, 0.023 mol) was added to the prepared solution and agitated with magnetic stirring to dissolve it. The solution was agitated all night to create a gel. After that, it was dried for 15 h at 60 °C in an oven. It was subsequently dried for 4 h at 120 °C. The obtained powder, which was yellow, was cleaned with ethanol and centrifuged multiple times at 3500 rpm until a clear supernatant was observed. It was then dried for a whole night at 70 °C in a vacuum oven. The powder that resulted was heated in air at 150 °C for 12 h, 250 °C for 4 h, 350 °C for 3 h, 450 °C for 2 h, 550 °C for 1 h, and 600 °C for 1 h. Each time the sample was heated, it was allowed to cool.

2.3. Method for the Preparation of Mesoporous Zirconia. Mesoporous zirconia (ZrO_2) was prepared as stated in the literature.[32,40] P-123 surfactant (5 g, 8.2×10^{-4} mol) was mixed in 1-butanol (56 g, 69 mL, 0.75 mol) and HNO_3 (8 g, 6 mL, 0.128 mol), which was contained in a 150 mL beaker. Zirconium butoxide (10 g, 0.026 mol) was then added and dissolved in the prepared solution at RT under a magnetic stirrer. The resulting transparent gel was dried for 4 h at 120 °C in the oven. After dividing the resulting greenish film/powder into three samples, it was immediately heated under air for 4 h at 450°, 3 h at 550°, and 1 h at 600°, all at the rate of 2 °C per minute. The hybrid ceria-zirconia was created using a different synthesis.

2.4. Preparation of Hybrid Ceria-Zirconia by the Inverse Micelle Method. 1-Butanol was combined with P-123 and nitric acid (which served as a water source) in a mass percentage ratio of 85:12:3. Consequently, a 150 mL beaker was filled with a mixture of 1-butanol (85 g, 1.15 mol), P-123 surfactant (12 g, 0.21×10^{-2} mol), and HNO_3 (3 g, 0.05 mol). Since there is a 2:1 ratio of salt to P-123, 24 g of zirconium butoxide and 24 g of cerium nitrate were added to the mixture and continually agitated overnight to ensure adequate homogeneity. The resulting gel was dried for 15 h at 80 °C in an oven. The resulting solid was dried for 3 h at 120 °C. After being ground into a fine powder and cleaning with ethanol, the resulting particles were left to dry overnight at 70 °C in a vacuum oven. The obtained powder, which was yellow, was subjected to baking cycles as in CeO_2. The catalysts are represented as $Ce_xZr_{1-x}O_2$ (x = 0, 0.2, 0.5, 0.8, and 1).

2.5. Catalyst Characterization. Using a sorption device called Micromeritics ASAP 2460 and the Brunauer–Emmett–Teller (BET) method, nitrogen sorption measurements were performed on the catalyst. Before the trials, the materials must be degassed for 18 h at 90 °C. The materials were subjected to X-ray diffraction (XRD) investigations using a diffractometer Rigaku MiniFlex-600 with Cu Kα radiation (λ = 0.1541 nm) to produce an XRD diffractogram at room temperature. Both low- and wide-angle diffraction patterns were observed at step rates of 0.015°/min and 0.1°/min, respectively. Using a J-J 2100F with a speed-up voltage of 200 kV, transmission electron microscopy (TEM) analysis was carried out for the morphology study. An Agor Turbo carbon coater was used to carbon-coat fresh samples on an aluminum stub for elemental composition analysis, which was then performed using scanning electron microscopy (SEM) equipment, equipped with an energy-dispersive X-ray spectroscopy (EDX) analysis system at a high voltage of 20 kV.

2.6. Catalytic Activities of Benzyl Alcohol Oxidation. Two-neck round-bottom flasks, each holding 25 mL of benzyl alcohol, were used for the catalytic oxidation process. The flasks were equipped with a reflux condenser and thermometer. The reaction was carried out by combining 0.15 g of catalyst ($Ce_{0.8}Zr_{0.2}O_2$), 30 mmol of benzyl alcohol, and 45 mmol of TBHP as the oxidizing agent. The formed mixture temperature was raised to 90 °C for 4 h while being vigorously stirred under reflux at 450 rpm. At several points, a portion of the mixture was pipetted and rapidly diluted with dichloromethane. After filtering, the diluted material was sent to a GC vial for quantification. The analysis was conducted using GC gas equipment, equipped with an FID, a capillary column, and N_2 as the carrier gas. The temperature of the FID was 370 °C, and the injection port was 200 °C. The following equations (eqs 4 and 5) illustrate how the yield/conversion and selectivity were determined using the FID data.

$$\text{Yield} = \frac{\text{change in } \textbf{benzyl alcohol} \text{ substrate concentration}}{\text{initial } \textbf{benzyl alcohol} \text{ substrate concentration}} \times 100\% \quad (4)$$

$$\text{Selectivity} = \frac{\text{con. of } \textbf{benzaldehyde} \text{ product}}{\text{total concentration of all products formed}} \times 100\% \quad (5)$$

2.7. Design of Experiment (DOE). *7.1. RSM Using the CCD for Benzyl Alcohol Oxidization.* The design of the experiment (DOE) process was used to examine the impact of

https://doi.org/10.1021/acsomega.4c02174
ACS Omega 2024, 9, 34464−34481

different input variables on the oxidation of benzyl alcohol to the benzaldehyde product from an aqueous solution. DOE is an optimization technique used to enhance process performances by examining the relationships between various input variable combinations and how these combinations affect the response of the process. This makes it possible to identify the most crucial input factors.[41] Response surface methodology (RSM) is an optimization tool used to optimize multiple input variables to achieve the optimal conditions of the variables whose interactions can offer maximum or minimum response within the region of interest.[42] RSM has several drawbacks, including its inability to predict results from systems that operate outside of its research scope, its unsuitability for extremely nonlinear systems, and its reliance on the potentially false assumption that there is a quadratic relationship between variables and responses. Despite these shortcomings, RSM is still a useful technique for optimization across a range of sectors. It is capable of generating a mathematical and statistical model that can be used to describe the reaction process.[43,44] Among different design types of RSM, CCD is the most popularly utilized. Their usage is because they make it possible to fully fit a second-order polynomial model to the data, thereby enabling the capturing of nonlinear relationships between the input factors and the output response. Additionally, it provides enough information to allow curvature analysis and the estimation of the main effects and their interactions.[45] Numerous practical studies have demonstrated that, in most cases, the optimum region may be satisfied with the quadratic model (or a higher-order polynomial).[46] Nonetheless, assessments of the link between input variables and responses can be made graphically using the response surface.[47] Hence, this experiment was designed using the central composite experimental design (CCD). In accordance with CCD, the minimum number of experiments required to effectively study the responses of any given input variables is given by the design equation (N) of eq 6[48,49]

$$N = 2^k + 2k + \mathrm{No} \tag{6}$$

where k is the number of input factors and No is the center point.

However, the design consists of 2^k factorial factors, which define the number of factorial points, enhanced by $2k$ axial factors, which were chosen at a distance of α from the design center,[42] and center factors, which help reduce the experimental error, as some experimental repetitions are necessary.[48,50] In addition, the factorial points showed equal variations between the low and high values (+1 and −1), while the axial points were chosen to be ($\alpha = \pm 1.68$) to ensure that the orthogonality and rotatability of each independent variable are measured at five levels of ($-\alpha$, −1, 0, 1, $+\alpha$).[36,51−56] Therefore, based on what we want to achieve, the range of values, actual and coded, were inputted into the statistical tool in such a way that their minima, central, and maxima values take the values of ($-\alpha$, 0, and $+\alpha$) (Table 1). The differences in axial points for each level divided by four give the incrementing value for each independent variable. Consequently, a total of 20 minimum experimental runs were designed, conducted, and systematized in a factorial design (eight factorial points, six axial points, and six center points). The experimental runs were randomized to eliminate systematic error. A second-order polynomial regression model, centered on a quadratic equation, with the response (Y),

Table 1. Independent Variables and Their Coding Levels for the Design of the RSM Experiment

	ranges & levels				
codes & parameters	$-\alpha$ (−1.68)	−1	0	+1	$+\alpha$ (+1.68)
A: catalyst amount (grams)	0.1	0.125	0.150	0.175	0.2
B: temperature (°C)	60	75	90	105	120
C: time (hours)	2	3	4	5	6

which is associated with the independent variables (eq 7), was utilized to fit the model during multiple regression analysis.

$$Y = \beta_o + \sum_{i=1}^{k} \beta_i x_i + \sum_{i=1}^{k} \beta_{ii} x_{ii}^2 + \sum_{i=1}^{k} \sum_{j=1}^{k} \beta_{ij} x_i x_j + \varepsilon \tag{7}$$

where Y represents the responses; k is the total number of independent variables; β is the intercept; i, ii, and ij with β represent the linear coefficient, quadratic coefficient, and interaction coefficient, respectively; xi and xj indicate the coded levels for independent variables; and ε is the statistical error.[57,58]

For further research, analysis of variance (ANOVA) was employed to evaluate the statistical significance of the components with respect to their contribution to the response values. ANOVA reveals any significant mismatch between the experimental data and the predicted data.[59] The model's acceptability was assessed using the F-value, the adequate precision value, P-values of the ANOVA, and the coefficient of regression (R^2). A lack-of-fit test was employed to evaluate the predictive models' suitability. In addition, the predicted error sum of squares (PRESS) is further used to evaluate the proposed quadratic model. Lower PRESS and higher R^2 with a large enough precision larger than 4 are indicators of a superior predictive model. However, the process optimization of the oxidation parameters using CCD−RSM followed six important steps. (1) Identifying the independent variables with their factorial and axial points: Three independent parameters were identified. They are the catalyst amount (A) (0.1−0.2 g reaction), temperature (B) (60−120 °C), and reaction time (C) (2−6 h) with constant 30 mmol of benzyl alcohol, 45 mmol of TBHP oxidizing agent, and rigorous refluxing of 450 rpm. (2) Possible experimental design using a central composite experimental design: In this research, 20 experimental trial runs were designed using the statistical software Design-Experts, Version-13. The CCD matrix consists of eight factorial points, six axial points, and six numbers of repetition. The remaining steps are (3) performing experiments as per design to obtain results; (4) recording the data from experimentation; (5) acquiring ANOVA results, computing the coefficients, and fitting the model equation; and (6) acquiring the optimal conditions.

2.7.2. Artificial Neural Network (ANN) Modeling. In contrast to RSM, ANN could generate an output by combining uncontrollable components.[60] It can be characterized as a tool that mimics the organizational principles of the human brain. However, a typical ANN topology consists of three layers: an input layer, a hidden layer, and an output layer.[38] The hidden layers link the inputs with the output layer and contain computational nodes called neurons.[61] These artificial neurons are regarded as strongly coupled processing units, having a summing junction and transfer functions. After processing the

https://doi.org/10.1021/acsomega.4c02174
ACS Omega 2024, 9, 34464−34481

signals from the input layer, a transfer function is used by the last hidden layer to transmit the processed data as an approximate output signal.[62] The term "network architecture" is used to refer to the pattern of interconnectivity among various neurons inside the artificial neural network (ANN) structure.[61] An essential part of designing the model is to determine how many neurons are in the hidden layer. The ANN model for the oxidation of benzyl alcohol was simulated using the neural network of MATLAB R2018b. The model was developed using a nonlinear relationship between the process input variables and the experimental benzaldehyde oxidation yield. A feed-forward propagation with a multilayered perception neural network is employed to forecast the outcome. However, 20 data sets that were used in the RSM were also utilized to ensure adequate modeling. Through trial and error, the optimal number of neurons for the hidden layer was determined, minimizing the error between the predicted and experimental values. This measure was implemented to prevent overfitting that is associated with either a big or small number of neurons.[38] The data set of the experimental yield is divided into a training data set, a testing data set, and a validation data set. The first step in the simulation process is network training, in which 70% of the training data sets were utilized to develop the relationship between the input and output functions. The rest 30% of the data set was subdivided into 15% testing data (used to check the overfitting of the data) and 15% validation data (used to check the error in the developed model). Therefore, the ANN model architecture employed in this study was 3−21−1, which corresponds to three input variables, 21 neurons in the hidden layer, and one output variable as shown in Figure 2b. To determine the degree of connection between the independent factors and the dependent component and to gauge the predictability of the ANN, the mean square error and the correlation coefficient were employed as performance checks.[36]

2.7.3. Adaptive Neuro-Fuzzy Inference System (ANFIS). ANFIS is a potent technique that essentially combines the best capabilities of fuzzy logic with artificial neural networks (ANNs). Hence, it provides a synergetic effect that incorporates the advantages of both systems in linear and nonlinear processes.[63] Generally, there is a prediction that ANFIS modeling is good when the number of input variables is not more than five.[64] If ANFIS inputs exceed five, the computational time and rule numbers will increase, so ANFIS will not be able to model the output with respect to the inputs.[65] As such, in this study, the number of input variables was three, including "catalyst amount, reaction time, and reaction temperature", thus supporting the model's application. The ANFIS model for the oxidation of benzyl alcohol was simulated using the fuzzy logic toolbox of MATLAB R2018b. This model is based on the Takagi−Sugeno inference system, which is governed by the IF-THEN rule.[66−68] As in ANN modeling, the ANFIS modeling process includes three categories: training, testing, and validation. Therefore, the training, testing, and validation stages are structured to have 70, 15, and 15% data sets of the experimental benzyl aldehyde yield. Before training, the data set is normalized to be in the range between 0 and +1 to decrease their range and increase the precision of the findings.[64] After the normalization process, the data became ready for the training process. Figure 2a depicts the ANFIS network architecture for the prediction of benzaldehyde yield, and it is equivalent to the first-order Sugeno-type inference system.[66] This architecture is structured

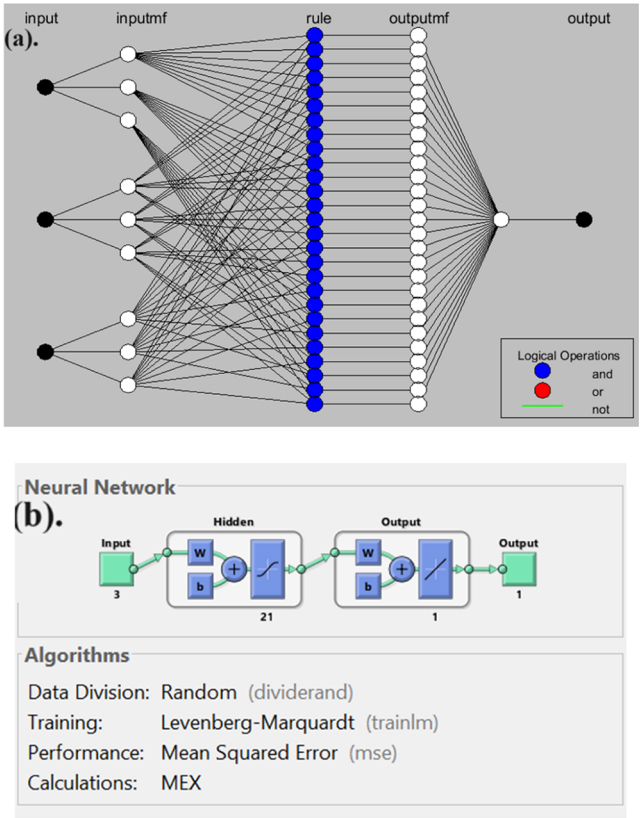

Figure 2. (a) ANFIS structure for benzaldehyde production showing five inputs and one output parameter. (b) Model architecture of the ANN (3:21:1).

into five layers, whose functions are fuzzification, multiplication, normalization, defuzzification, and summation. The first layer of the model, fuzzification, contains the input variables and their membership functions (MFs). MF permits tuning as a measure to improve computation accuracy with a minimum error.[69,70] To simulate the data sets for optimal ANFIS model prediction and fuzzy inference system (FIS) generation, grid partitioning with an input number of membership functions (MFs = 3, 3, and 3) as well as input and output membership functions of types of "trimf" and "constant", respectively, was selected, and the hybrid optimization method was used to train the FIS with an error tolerance of zero.[71]

2.7.4. Assessment of the Developed Models. Error statistical analysis is a viable method used for the assessment of the models. Seven standard error statistical functions as provided in the Supporting Information of equations (eqs S1−S6) were used for comparing the applicability of the developed models. They include mean squared error (MSE), root-mean-square error (RMSE), mean absolute percentage error (MAPE), mean relative percent deviation (MRPD), hybrid fractional error function (HYBRID), Marquardt's percent standard error dev. (MPSED), and coefficient of determination (R^2). Exceptional model performance is achieved in the structure when the MSE and RMSE approach 0 and the R^2 value approaches 1. In addition, a comparison plot displaying the three models would be used to show the deviations of the model-output predictions from the experimental output.

2.8. Reusability of Catalysts. The ability of heterogeneous catalysts to be recycled for reuse represents one of their

https://doi.org/10.1021/acsomega.4c02174
ACS Omega 2024, 9, 34464−34481

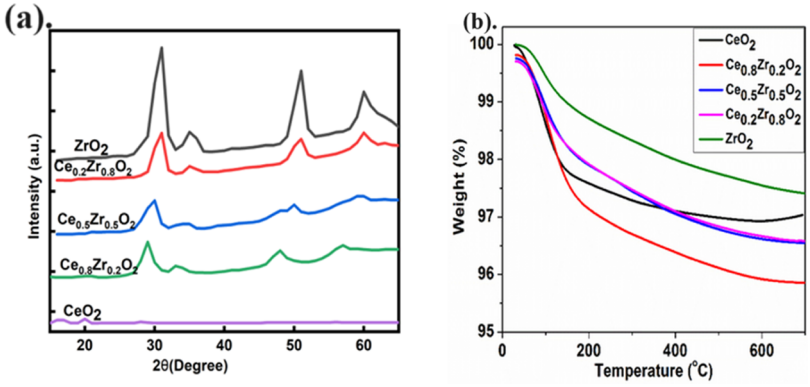

Figure 3. (a) XRD patterns of mesoporous $Ce_xZr_{1-x}O_2$ calcined at 450 °C. (b) Thermogravimetric analysis (TGA) curves of mesoporous $Ce_xZr_{1-x}O_2$ materials calcined at 450 °C.

Table 2. Physicochemical Properties of Mesoporous Catalysts Calcined at 450 °C

samples	surface area ($m^2\ g^{-1}$)	pore diameter (nm)	pore volume ($cm^3\ g^{-1}$)	crystallite size (nm)	total basicity × 10^2 (mmol $CO_2\ g^{-1}$)
1. CeO_2	117	5.10	0.12	7.65	62
2. $Ce_{0.8}Zr_{0.2}O_2$	165	8.23	0.27	4.42	125
3. ZrO_2	101	3.17	0.10	8.02	52

primary advantages. The reusability of the $Ce_{0.8}Zr_{0.2}O_2$ catalyst synthesized by the inverse micelle method was investigated for three conservative cycles under ideal optimal conditions, which included 0.16 g of catalyst, 94.5 °C for the reacting temperature, with 30 mmol of benzyl alcohol, 45 mmol of TBHP oxidizing agent, and rigorous refluxing of 450 rpm after 4.2 h of reaction time. To be employed again in another reaction cycle, the catalyst must be washed after each run, dried, and calcined at 450 °C for 12 h.

3. RESULTS AND DISCUSSION

3.1. Characterization of the Catalyst. *3.1.1. XRD Analysis.* The crystallinity of the obtained ceria-zirconia catalyst ($Ce_xZr_{1-x}O_2$) was tested with an XRD instrument. Pure mesoporous ceria (CeO_2) (JCPDS card 49-1642) exhibit peaks that are characteristically indicative of a cubic fluorite structure, as shown in Figure 3a. As the dosage of zirconia rose, the intensity of the diffraction peaks became more significant. Hence, the characteristic of a cubic fluorite structure was also seen in mixed cerium nanoparticles ($Ce_xZr_{1-x}O_2$). These distinct peaks corresponded to (111), (200), (220), (311), (222), and (400) planes, respectively, at 2θ = 28.5, 33.0, 47.5, 56.4, 59.1, and 69.4°. Consequently, the persistency of the fluorite structure in the mixed catalyst is responsible for its enhanced oxygen storage capacity (ORC).[72] Conversely, a tetragonal-shaped peak is seen at 2θ = 30.7°, 35.6° (200), 50.9°, 60.5°, and 63.1° for both pure zirconium (ZrO_2) and mixed cerium nanoparticles ($Ce_{0.2}Zr_{0.8}O_2$). This peak corresponds to the planes (111), (220), (311), (220), (311), and (222). Furthermore, the positions and intensities of the generated peaks match the structure of the cubic fluorite described by Faqeeh et al.[73] The observed phase disparity in the prepared composite suggested the successful formation of cerium cubic crystals in the structure of ZrO_2. The diffractogram of the mixed catalyst indicated that smaller Zr^{4+} species were appropriately incorporated into the larger crystal framework of CeO_2. Therefore, the structural changes of the cubic fluorite lattice, which improves thermal stability, resistance to sintering, and oxygen storage capacity, are caused by the insertion of smaller zirconia cations into the ceria crystal lattice.

3.1.2. TGA Analysis. In another development, TGA was conducted on the as-synthesized ceria-zirconia catalyst ($Ce_xZr_{1-x}O_2$) to study its transformational behavior as heat flows into its structure. The TGA curve, as seen in Figure 3b, demonstrates two stepwise decompositions: a considerable weight depreciation between 140 and 179 °C and a slow weight loss from 200 to 600 °C. The considerable weight loss may be due to the evaporation or elimination of strongly adsorbed amounts of water molecules. Thereafter is the region where minimal weight loss is observed. This characteristic indicates thermal stability, implying that the substance will maintain its stability at elevated temperatures. Therefore, residual volatiles, the oxygen loss from CeO_2 at high temperatures, and the burning and oxidation of nitrogen compounds, likely from the incomplete combustion of the cerium precursor, can be blamed for the mass loss in general.[74−76]

3.1.3. BET Analysis. The specific surface area (SSA) and pore structure of the synthesized ceria-zirconia solid solutions at 450 °C were investigated using a BET measurement, as shown in Table 2. Compared to pure zirconia or pure ceria, the generated ceria-zirconia solid solutions showed comparatively large specific surface area values (101−165 m^2/g) and high total pore volumes (0.10−0.12 cm^3/g). As a result, $Ce_{0.8}Zr_{0.2}O_2$'s surface area increases when CeO_2 is modified with Zr, reaching a maximum value of 165 $m^2\ g^{-1}$ as opposed to CeO_2's 117 $m^2\ g^{-1}$. The largest SSA of $Ce_{0.8}Zr_{0.2}O_2$ nanostructures could be attributed to their smallest crystallite size (4.42 nm), the good distribution of the active metal nanoparticles, and their strong coupling effect with the oxide support.[77] The surface mesostructured enhancement of pure ceria following the incorporation of zirconium into its lattice structure can significantly alter the catalytic efficiency of the mixed mesoporous materials. A comparable pattern was noticed in the structure, where the ceria-zirconium catalyst synthesized with the largest specific surface area (84 $m^2\ g^{-1}$) also had the smallest average crystallite size (8.2 ± 0.4 nm).[78]

https://doi.org/10.1021/acsomega.4c02174
ACS Omega 2024, 9, 34464−34481

Therefore, it seems that adding metal particles to a material's microporosity improves its surface area. On the other hand, the porosity of the as-synthesized catalyst ($Ce_{0.8}Zr_{0.2}O_2$) was investigated using nitrogen adsorption−desorption isotherms. The obtained hysteresis loop as shown in Figure 4 is a classical

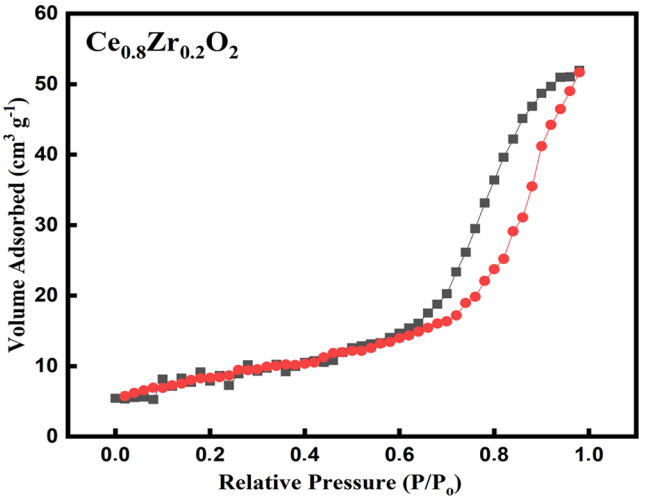

Figure 4. Isotherm profile of the mesoporous $Ce_{0.8}Zr_{0.2}O_2$ calcined at 450 °C.

type IV adsorption−desorption isotherm, which is characteristic of mesoporous materials.[79] As can be seen, the evolution of the hysteresis loop increases in the adsorption region at a relatively higher pressure (P/P_0). Therefore, it is comparable to type III isotherms with a type-H3 hysteresis loop. This is an indication of mesoporous structures that are moderately organized and contain aggregates of nonrigid nanoparticles.[80,81]

3.1.4. TEM, EDX, and SEM Analyses. To gain an understanding of the morphology and particle size distribution of the high-efficiency catalyst ($Ce_{0.8}Zr_{0.2}O_2$), TEM analysis was conducted. Figure 5a shows the TEM image of the catalyst calcined at 450 °C. As can be seen from Figure 5a, the catalyst displays uniformly distributed, spherically shaped nanoparticles formed by agglomeration. The catalyst's TEM image is morphologically consistent with the one that Cao and colleagues[79] acquired when examining CO oxidation using a synthetic $Ce_{0.8}Zr_{0.2}O_2$ catalyst. Conversely, Figure 5b displays the SEM image of the catalyst ($Ce_{0.8}Zr_{0.2}O_2$), synthesized by the inverse micelle method. The imagery shows that the nanoparticles are agglomerated and porous, conforming to TEM analysis. Inhomogeneous structures were also observed in the imagery, and this is a common phenomenon observed in solid solutions over time. Hence, the growth in the crystal size of ceria-zirconia can be explained using the Ostwald ripening phenomenon, whereby the smaller crystal species will diffuse to larger crystals, allowing the larger crystals to grow at the expense of the smaller ones.[82,83] Additionally, Figure 5c represents the EDX elemental analysis attesting to the purity of the synthesized catalyst, thereby supporting the XRD pattern, which displays a lack of an impurity signal. The EDX spectral analysis confirms the presence of cerium, carbon, oxygen, and zirconium with atomic weight percentages of 48.7, 21.8, 16.7, and 12.8 wt %, respectively. The presence of carbon on the catalyst surface was from the sample preparation carbon coater. The average particle size of the catalyst as displayed in the particle size distribution histogram (Figure 5d) is 24.5 ± 1.7 nm, and this is in good agreement with the XRD result.

3.2. Influence of Operating Parameters Using Three-Dimensional (3D) RSM Plots. The benefit of using RSM is that it can be used to create a 3D response plot that helps identify how interactions between process factors affect the process outcome. Each plot illustrates the impact of two variables while holding the others constant.

Figure 6a surface plot shows an increment in benzyl alcohol conversion from 88.5 to 98.6% at a lower reaction temperature of 75 °C when the catalyst amount is increased from 0.125 to 0.155 g. This increase could be attributed to the availability of more active locations on the surface of the catalyst. It was observed that a further increase in the mass of the catalyst to 0.175 g results in a slight decrease of the benzaldehyde yield to 95.1%. The decrease in benzaldehyde yields may be due to the excess catalyst, which increases the resistance to mass transfer, causing a decrease in the reactant mobility toward the active sites. Too many catalysts that are in excess can develop the selectivity of benzoic acid.[84]

Figure 6b showcases the combined effect of the mass of the catalyst ($Ce_{0.8}Zr_{0.2}O_2$) on the yield with respect to reaction time. However, in the absence of a catalyst, conversion to benzaldehyde was sluggish with respect to reaction time. Selectivity for benzoic acid increases with a decrease in benzaldehyde formation. However, an increase in the mass of the catalyst from 0.125 to 0.155 g at 75 °C resulted in a slight increase in the yield of benzaldehyde from 88.5 to 97.5%. An excess amount of catalyst increases the selectivity of benzoic acid, and this was attributed to the fact that the excess catalyst containing active Lewis acid sites can accelerate further the oxidation of benzaldehyde into benzoic acid.[85] Similar trends were observed by Choudhary et al.,[86] who concluded that benzyl alcohol oxidation is a heterogeneous reaction.

On the other hand, Figure 6c displays the combined effect of reaction temperature with time on the yield of benzaldehyde. However, when the temperature of the reaction mixture rises, the molecules' kinetic energy increases, increasing the output of benzaldehyde. The figure reveals that the yield will decrease slightly from 98.6 to 92.1% with respect to the time when the reacting mixer is heated to 90 °C and then raised to 105 °C. As a result, at elevated temperatures, the yield of benzaldehyde drops with respect to an increase in reaction time. Hence, heating the reacting mixtures to 90 °C for 4 h gives the maximum yield of 98.6%. The yield of benzaldehyde drops with increasing temperature and reaction time after 4 h of reaction. However, different loadings of ZrO_2 into the lattice structure of CeO_2 were prepared originally. The catalyst $Ce_{0.8}Zr_{0.2}O_2$ was used throughout this experiment. This is because $Ce_{0.8}Zr_{0.2}O_2$ produces the maximum benzaldehyde yield for 4 h, after which it decreases slightly. The breakdown of TBHP appears to be the catalyst's first activity in the benzyl alcohol oxidation. As a result, extremely reactive atomic oxygen species were created, which caused benzyl alcohol to be oxidized into benzaldehyde. The catalytic activity of the ceria lattice for the oxidation of benzyl alcohol is greatly increased upon the addition of the zirconia molecule.

3.2.1. ANOVA and RSM Analyses. The experiments performed with the central composite design of RSM were to examine how the independent variable affected the benzyl alcohol oxidation efficiency corresponding to the benzaldehyde yield. The yield of the oxidation process, as a response function, and the complete factorial design matrix for the

https://doi.org/10.1021/acsomega.4c02174
ACS Omega 2024, 9, 34464−34481

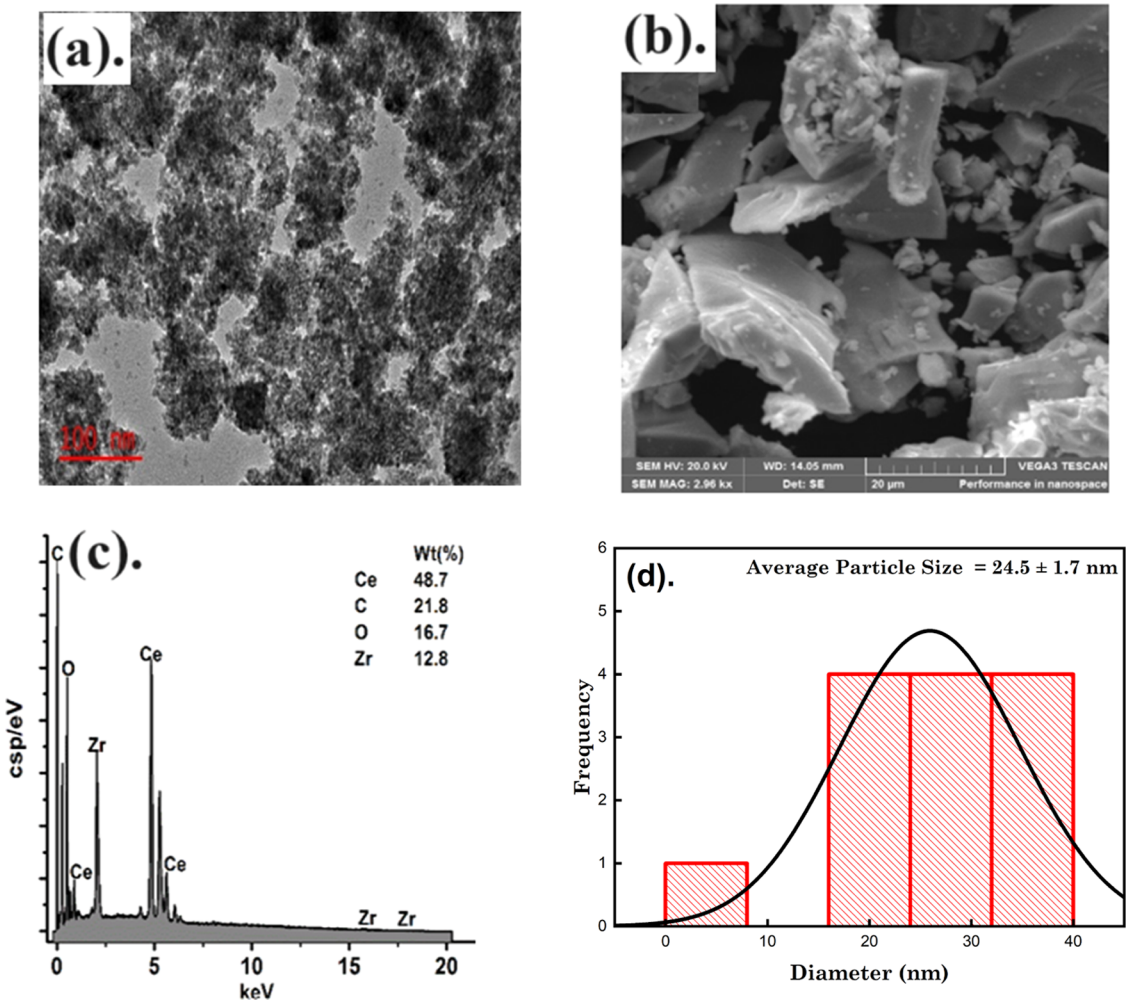

Figure 5. (a, b) TEM and SEM images of $Ce_{0.8}Zr_{0.2}O_2$ calcined at 450 °C. (c) EDX of $Ce_{0.8}Zr_{0.2}O_2$ calcined at 450 °C. (d) Particle size distribution of the SEM image.

experimental runs using CCD-RSM are shown in Table S1. However, Table 3 displays the results of the analysis of variance (ANOVA) for benzyl alcohol oxidation. The *F* and *p*-values (probability value) of the variables were used to define the significance and magnitude of the model coefficient terms. Using a 95% confidence level, as the foundation for evaluating the significance of the oxidation process, *p*-values of more than or equal to 0.05 are considered insignificant; otherwise, they are considered significant.[87,88] The linear terms *A* (amount of catalyst), *B* (reaction temperature), and *C* (reaction time), the collaborating terms of AB and BC; and the pure quadratic terms A^2, B^2, and C^2 are designated as significant. On the other hand, the model term AC was statistically insignificant. As a result, the developed model with the elimination of the insignificant term was reduced, and this helped improve and simplify it. Hence, eq 8 represents the quadratic polynomial model equation generated for benzyl alcohol oxidation with respect to the input variables, excluding the nonsignificant term. In general, a low *P*-value of <0.0001 was observed with the model, and this indicates model significance.

$$\text{Yield} = 98.0294 + 0.71925 \times A + 1.3493 \times B + 0.939248 \times C - 0.5125 \times AB + 0.6375 \times BC - 1.27669 \times A^2 - 2.28431 \times B^2 - 2.77929 \times C^2 \quad (8)$$

where *A*, *B*, and *C* represent catalyst amount, reaction temperature, and reaction time, respectively.

Furthermore, Ahmadi et al.[89] stated that lower *P*-values (<0.05) and higher *F*-values are characteristic of a highly significant model. Therefore, the ANOVA result of Table 3 indicates that the model is highly significant, as evidenced by the high *F*-value of 87.72 and the lower *p*-value of less than 0.0001. However, the purpose of the derived formula (eq 8) is to calculate the yield efficiency of benzaldehyde generation by the oxidation process of converting benzyl alcohol with TBHP. Finding the factors' respective impacts can be accomplished by comparing their factor coefficients. Model terms with a positive coefficient demonstrated a synergistic effect, whereas one with a negative coefficient demonstrated an antagonistic effect.[43] This means that the oxidation of benzyl alcohol to benzaldehyde is favored by an increase in the model terms with positive signs.

Also, a high coefficient of determination (R^2) guarantees that the second-order quadratic model fits the experimental data well, hence confirming its reliability. In addition, a very strong R^2 of the experimental and predicted values indicates a well-fitted design matrix. The fit statistics of benzyl alcohol oxidation of Table 4 indicate a high R^2 value of 0.9875, adjusted R^2 of 0.9762, and a predicted R^2 of 0.9320 for the model. The R^2-adjusted value is close to R^2. Statistically, the

https://doi.org/10.1021/acsomega.4c02174
ACS Omega 2024, 9, 34464−34481

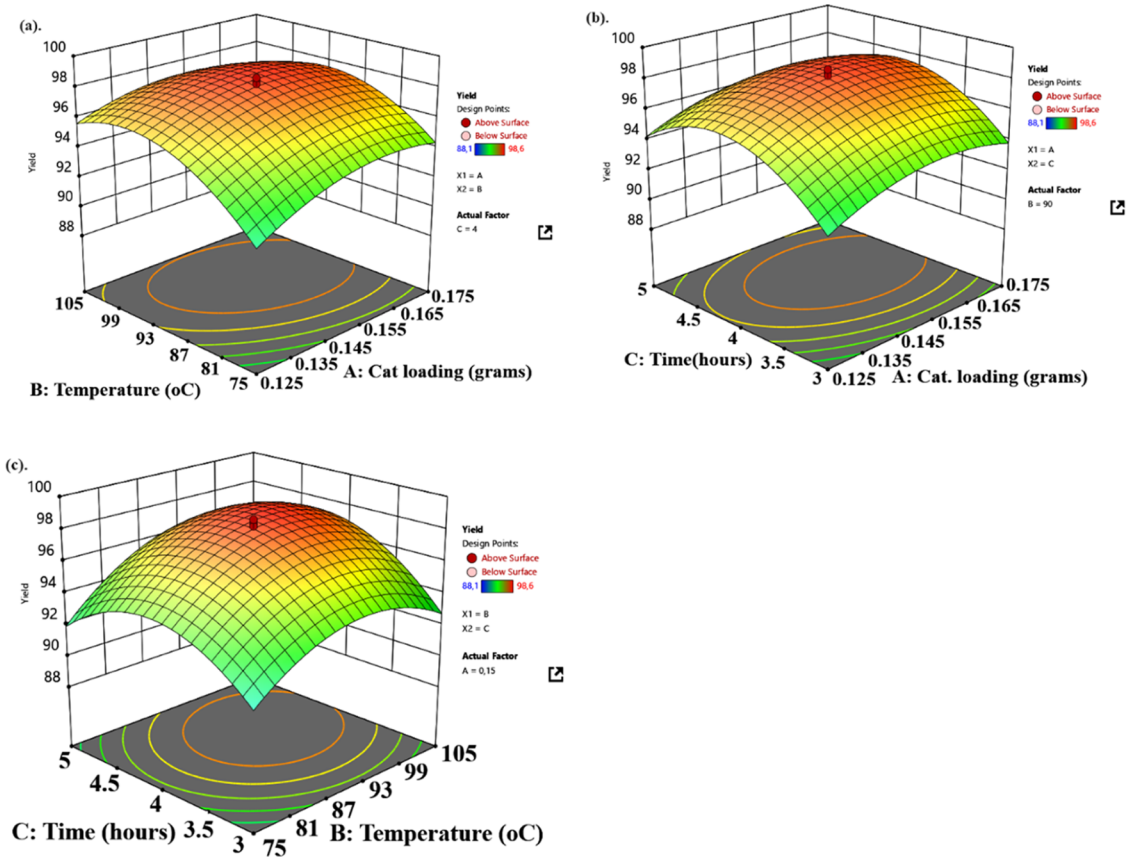

Figure 6. (a) Effect of catalyst amount. (b) Effect of catalyst amount and time. (c) Effect of temperature on benzaldehyde yield.

Table 3. ANOVA Fit of Benzyl Alcohol Oxidation Using the CCD-RSM Model

source	sum of squares	df	mean square	*F*-value	*p*-value	
model	229,24	9	25,47	87,72	<0.0001	significant
A-cat. loading	7,06	1	7,06	24,33	0,0006	
B-temp	24,86	1	24,86	85,63	<0.0001	
C-time	12,05	1	12,05	41,49	<0.0001	
AB	2,10	1	2,10	7,24	0,0227	
AC	0,0313	1	0,0313	0,1076	0,7496	
BC	3,25	1	3,25	11,20	0,0074	
A^2	23,49	1	23,49	80,90	<0.0001	
B^2	75,20	1	75,20	258,99	<0.0001	
C^2	111,32	1	111,32	383,38	<0.0001	
residual	2,90	10	0,2904			
lack of fit	1,83	5	0,3661	1,71	0,2862	not significant
pure error	1,07	5	0,2147			
cor total	232,14	19				

difference between predicted R^2 and adjusted R^2 should be less than 0.2.[90,91] As can be observed, the difference between the predicted R^2 and the adjusted R^2 was 0.0442, and this indicates that the model fits the experimental data and may be used for interpolation with reliability. Adequate precision ratio is a measurement of the signal-to-noise ratio, and a considered value greater than or equal to 4 is always desirable.[92] A value of 24.777 obtained in this analysis suggested adequate model efficacy.[93] On the other hand, a comparatively low coefficient of variance (CV) value of 0.5751% was obtained. This implies good reliability and precision of the runs. It also shows that the model was highly functional, reproducible, and dependable.[94]

From the lack-of-fit test results of Table 5, the lack-of-fit *p*-value obtained is 0.2862, and this is more than 0.05, which is an indication that the model's lack of fit is insignificant, i.e., data fit well with the model. Therefore, a nonsignificant lack-of-fit indicates that the model and the experimental data points have a good match and are complementary. The *p*-value (0.2862) is greater than the significance level (0.05), indicating that there is no lack of fit in the model. Consequently, benzaldehyde yield was significantly predicted by the quadratic model using the input variables.

To validate the model's accuracy and adequacy, residual analysis was performed[95] and presented in the diagnostic plots as shown in the Supporting Information of Figure S1a–c.

https://doi.org/10.1021/acsomega.4c02174
ACS Omega 2024, 9, 34464−34481

Table 4. Fit Statistics of Benzyl Alcohol Oxidation

source of variation	regression
sum of squares	229.24
degrees of freedom	9
mean square	25.47
F-value	87.72
P-value	<0.0001
R^2	0.9875
adjusted R^2	0.9762
predicted R^2	0.9320
adeq precision	24.777
std. dev.	0.5389
mean	93.70
C.V.%	0.5751

However, deviations between the experimental responses and predicted values are known as residuals. The normal plot of residuals (externally Studentized residual against normal % probability), as indicated in Figure S1a, was appropriate for outlier detection and showed good conformance because the formed line was linear. Additionally, Figure S1b shows the graphical plot of the experimental and predicted response values for benzyl alcohol oxidation. This plot (Figure S1b) fitted well with linear regression, indicating that the model was adequate in describing the experimental terms. About the line of unit slope, it was observed that all data were logically spaced and close to one another. This excellent relationship validates the significance of the model as demonstrated by the orderliness between the expected and experimental data.[96] On the other hand, the residual plot vs run number is displayed in Figure S1c. The random residual plot confirms that all data points fall within acceptable bounds. None of the points were standing away from the red threshold, which is considered to be outside the limit of the model expectations.[97,98] This behavior also demonstrates the model's validity and accuracy. Based on the diagnostic plots of residual analysis, one can judge that the developed quadratic model captures the correlation between the responses and process variables successfully.

The perturbation plot as indicated in the Supporting Information of Figure S2 was utilized to compare the effect of all of the parameters, affecting the oxidation process of benzyl alcohol on a single plot.[99] Plotting was done to evaluate the response behavior resulting from the departure from the center point. In addition, the perturbation plot reflects the yield's departure from the reference point due to the independent variables. In this study, the reference points taken into consideration for the perturbation plot were 0.15 g of catalyst amount, 90 °C for the reaction temperature, and 4 h of reaction time. However, in the perturbation plot, the higher the sensitivity of the response toward the factor, the steeper the slope.[100] Based on this interpretation, from the perturbation plot, it was evident that *B* (reaction temperature) mostly affected the oxidation process, followed by factor *C* (reaction time) and then *A* (mass of the catalyst). Hence, selective benzaldehyde response was highly sensitized by the perturbation plot for a better understanding of the effect of the independent variables.

To find the optimum conditions for benzaldehyde yield, a numerical optimization process was conducted by permitting the criteria of all of the independent variables to be in range to maximize the yield. The Ramp plot for desirability analysis as presented in Figure S3 was employed to approximate the best predicted possibilities for the maximum response.[52] As indicated in the ramp's desirability plot, the optimal value of each parameter is shown by a red dot. The optimization of the process variables based on their response goal varies, from a desirable function (DF) of 0 (undesirable) to 1 (desirable). A DF of 1 indicates the response reaches its goal, while a 0 indicates that one or more data sets are beyond the specified bounds. The desirability function value obtained for the optimum yield of benzaldehyde was found to be 98% when 0.16 g of catalyst, 94 °C reaction temperature, and under 4.2 h of reaction time were used at constant 30 mmol of benzyl alcohol, constant 45 mmol of TBHP oxidizing agent, and rigorous refluxing of 450 rpm. The desirability of 0.98 means that the oxidation process achieved its goal. Hence, it can be concluded that the optimal reaction parameters for the oxidization reaction of benzyl alcohol over ceria-zirconium ($Ce_{0.8}Zr_{0.2}O_2$) were 0.16 g of catalyst, 94 °C reaction temperature, and under 4.2 h of reaction time with constant 30 mmol of benzyl alcohol, 45 mmol of TBHP oxidizing agent, and rigorous refluxing of 450 rpm.

3.3. Artificial Neural Network (ANN) Modeling.

MATLAB R2018b was utilized to conduct the ANN machine-learning model of benzyl alcohol oxidation to benzaldehyde yield. The output parameter was predicted by the feed-forward network using the Levenberg−Marquardt algorithm approach. Figure 2b shows the constructed and simulated ANN architecture consisting of three input neurons (representing independent parameters), 21 hidden neurons, and one output cell (representing the output value) called responses. The experimental output from 20 data sets was used to train the ANN, which then predicted the output for additional inputs. Three portions of data sets were created: 14 for training, 3 for validation, and 3 for testing. The coefficient of determination (R^2) values for testing, validation, and training as indicated in the ANN regression plot of Figure 7 were 0.96939, 0.92407, and 0.99808. These values showed that the benzaldehyde yield as predicted by the ANN model and the experimental data correlated strongly. Additionally, the total model plot of Figure 7 indicated a correlation coefficient (R^2) of 0.96775, demonstrating that the projected yield successfully tracked the experimental data. Excellent findings are shown in the four plots, with an R^2 value greater than 0.92. As a result, the correlation coefficients for each set of data were

Table 5. Lack of Fit Tests

source	sum of squares	df	mean square	*F*-value	*P*-value	
linear	187.09	11	17.01	79.23	<0.0001	
2FI	181.71	8	22.71	105.81	<0.0001	
quadratic	1.83	5	0.3661	1.71	0.2862	suggested
cubic	0.0469	1	0.0469	0.2184	0.6599	aliased
pure error	1.07	5	0.2147			

https://doi.org/10.1021/acsomega.4c02174
ACS Omega 2024, 9, 34464−34481

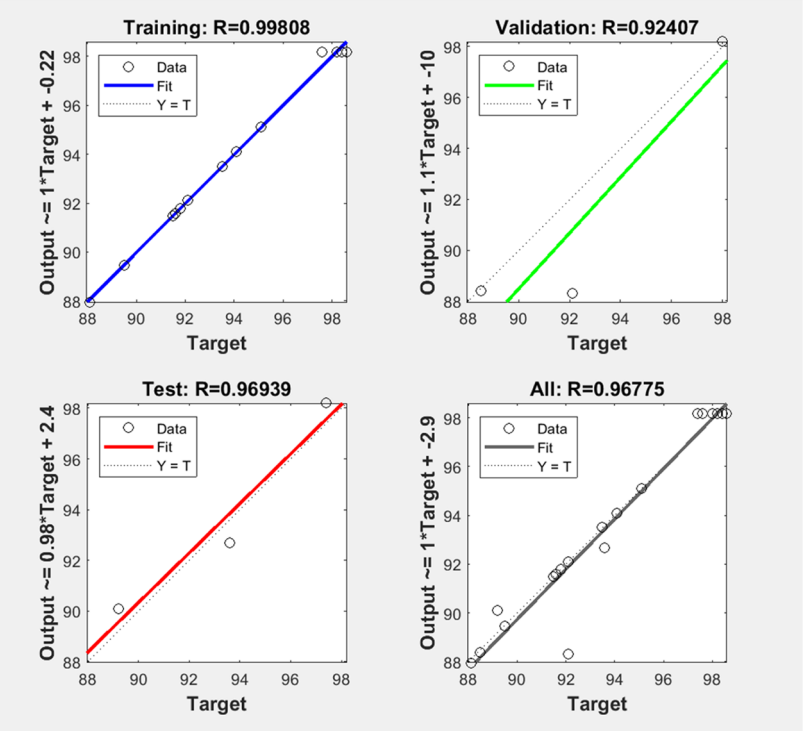

Figure 7. ANN regression plots for (a) training, (b) validation, (c) testing, and (d) overall oxidation process.

close to 1, indicating that the fit was appropriate. Another conclusion that might be drawn is that the neural network model's architecture produces good linearity with the desired values. Specifically, for the training and overall data sets, where the objectives were almost identical to the network outputs, the drawn line of best fit is almost on the 45° line. As a result, the oxidation reaction of benzyl alcohol to benzaldehyde could be adequately described by the artificial neural network output response. However, the performance plot, as seen in Figure S4a, with four epoch iterations was utilized to assess how reliable the neural network's training procedure was. Based on this model, the best validation performance was recorded at epoch 2, with a value of 4.8321, where the characteristics of the test set error and validation set error are similar. This is consistent with the results of Yadav et al.[101] obtained during the prediction of solar radiation using the ANN model. On the other hand, the error histogram plot of the discrepancies between target and forecast values may be found in Figure S4b. The network's performances are further verified using this graphic. Given that the error histogram displays the differences between the targeted and predicted values, the errors could be negative.[102] Training data is represented by the blue bar, validation data by the green bar, and testing data by the red bar. On the graph, bins represent the number of vertical bars. The number of samples from the data set that fall into a specific bin is shown on the *Y*-axis. The resulting histogram clearly shows outliers or areas of the data where the fit is noticeably poorer than the rest of the data. However, the zero-error value, which is located on the *X*-axis, is what the zero-error line alludes to. With reference to this plot, the feed-forward model has a bin at 0.07488 that corresponds to the zero-error point.

3.4. Adaptive Neuro-Fuzzy Inference System (ANFIS) Modeling. The ANFIS model was successfully implemented using the hybrid learning approach with a toolbox called MATLAB R2018b. The model is configured with three input parameters (the catalyst amount, the reaction temperature, and the reaction time) and an output that is regarded as the benzaldehyde yield. The grid partition employed is the fuzzy interference system (FIS) with the Sugeno architecture, as represented in the Supporting Information in Figure S5a. To generate a fuzzy logic for the 20 data sets, three MFs were assigned to each element of the input variables. A triangular-shaped (trimf) membership function (MF) was selected in the grid partition check for the modeling. The choice of triangular MF is because it produced the best results. Similarly, linear MF provides a better performance prediction. The output MF types of "constant" were chosen to create a more precise model for the FIS. With a 0% error tolerance, 200 epochs of iteration were used to train the FIS data set as shown in the ANFIS distribution plot for the trained data set (Figure S5b). The dotted and asterisk points denote the predicted and actual values. After two epochs of training with triangular MF, an RMSE error of magnitude 0.231661 was attained. This confirms that the fuzzy network was a good fit for simulating the oxidation of benzyl alcohol to aldehyde over a ceria-zirconium catalyst. Generally, the attributes of the obtained ANFIS model are showcased in Table 6.

Also, presented in Figure S6a−c are the ANFIS 3D surface plots illustrating the impact of two-factor interactions on the % yield of benzaldehyde. The benzyl alcohol oxidation to benzaldehyde was shown to peak with the maximum yield, for 4 h of reaction time, after which the yield decreases. As indicated in the optimization rule viewer plot of Figure S6d, an optimum benzaldehyde yield of 98% was recorded under the operating conditions of catalyst amount (0.15 g), reaction time (4 h), and reacting temperature (90 °C), with all of the other factors remaining constant. This clearly indicated that the results obtained through the ANFIS model were in good agreement with the RSM model.

https://doi.org/10.1021/acsomega.4c02174
ACS Omega 2024, 9, 34464−34481

Table 6. ANFIS Information Used in This Study

ANFIS parameters	
membership function type	Sugeno
output membership function	linear
number of nodes	78
number of linear parameters	27
number of nonlinear parameters	27
total number of parameters	54
number of training data pairs	20
number of fuzzy rules	27
ANFIS training completed at epoch	2
minimal training	RMSE = 0.231661

3.5. Comparison Performance between RSM ANN and ANFIS Model. Using performance indicators like R, R^2, and adjusted R^2 of the models and statistical error functions such as MSE, RSME, MAPE, MRPD, HYBRID, and MPSED, the efficiencies of the developed models (ANFIS, ANN, and RSM), in predicting the oxidation of benzyl alcohol to benzaldehyde, were evaluated. It can be observed from the parity plot of Figure 8 that ANFIS, RSM, and ANN recorded high values of R, which were 0.99769, 0.99372, and 0.96775. To achieve a good correlation and quality fit between the experimental and predicted values, the R value should be very close to unity. In addition, high R^2 and adjusted R^2 values for ANFIS, RSM, and ANN which were also obtained from the parity plot were (0.99538 and 0.99512), (0.98748 and 0.98679), and (0.93653 and 0.93301) respectively. All obtained R^2 values were higher than 0.93. This is an indication that more than 93% of the predicted data set fits within the line of best fit and is relatively close to the experimental values. However, the observed high values of R, R^2, and adjusted R^2 are indicative of the good fit of the models.[103] For a model to be adjudged reliable and acceptable, its R^2 value must be greater than 0.8.[36,53] Consequently, the adjusted R^2 was used to check the overestimation of the R^2. The obtained adjusted R^2 values were sufficiently very close to R^2, which further validated the correctness and accuracy of the predicted models.[104] However, ANFIS has the highest R and R^2 value and therefore gives a better correlation and prediction than RSM and ANN.

Furthermore, the model residual values that were calculated by taking the basic difference between the experimental data and the model's predictions as indicated in the Supporting Information Table S2 were used to compare model efficiencies. In the majority of the experimental runs, all three models produced modest residuals. The greatest negative and positive residues of (−0.89698) and (3.80074) were found under the ANN model. A low range of residual fluctuations, dispersed along the horizontal x-axis, indicates a better performance. ANFIS and RSM appeared to be the most suitable models due to their limited residual fluctuation along the x-axis (Figure 9a). However, it is crucial to note that ANN is the least accurate, as indicated by its high residual deviations, particularly in run number 13.

Also, the equations as presented in the Supporting Information (eqs S1−S6) were used to statistically calculate the error functions and were utilized to quantify and compare the efficiencies of the developed models. Their overall comparison is summarized in Table 7. Low magnitude in error values indicates better predictive capacity.[105] MSE, which is a measure of how close a fitted line is to a data point, was

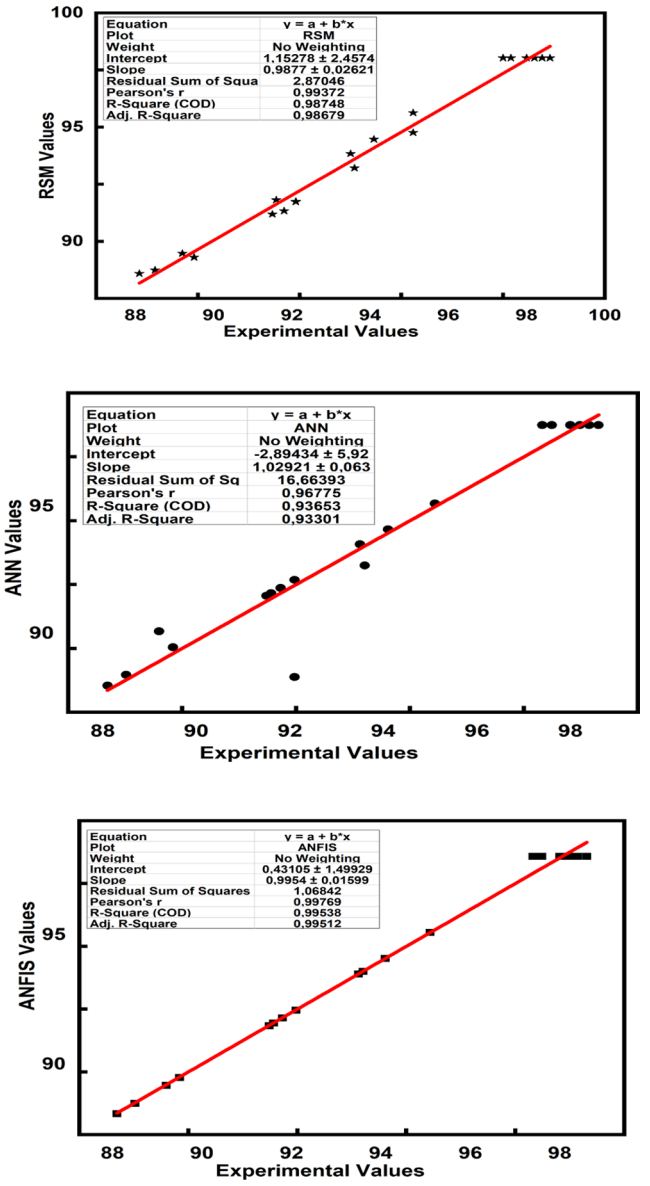

Figure 8. Parity plot between experimental and predicted values of (a) RSM, (b) ANN, and (c) ANFIS.

determined for the three models. In addition, the RMSE, which is the square root of the MSE, was also calculated. As observed from Table 7, the values obtained for both MSE and RMSE for ANFIS, RSM, and ANN were (0.05367, 0.23166), (0.14528, 0.38116), and (0.86779, 0.93155). These values were low, supporting the good fit of the models. On the other hand, MAPE, MRPD, HYBRID, and MPSED measure the accuracy and precision of a model.[106] Their obtained values for ANFIS, RSM, and ANN were (0.00588, 0.00286, 0.00337, and 0.00000001735), (0.01889, 0.00775, 0.00912, and 0.00000002855), and (0.02183, 0.04659, 0.05448, and 0.00000009864) as presented in Table 7. These values are also low, indicating the reliability and predictive accuracy of the three models. Considering the statistical results obtained in this work, the ANN model was the least efficient in terms of precision and accuracy in estimating the benzaldehyde yield, while the ANFIS model was better than the ANN model. The structure where the error value approaches zero (0) and the superlative R^2-value is near 1 is the acceptable exceptional

https://doi.org/10.1021/acsomega.4c02174
ACS Omega 2024, 9, 34464−34481

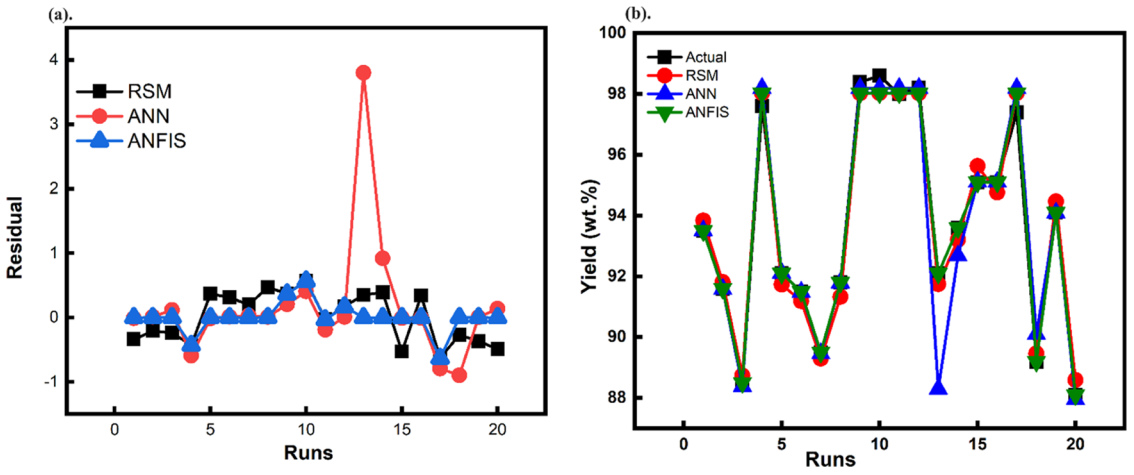

Figure 9. (a) Residual plot of RSM, ANN, and ANFIS model. (b) Comparison of experimental yield for benzaldehyde production with those predicted by RSM, ANN, and ANFIS.

Table 7. Statistical Error Analysis of the ANFIS, ANN, and RSM Models, Associated with the Comparison Plot

	results		
error function	ANN	RSM	ANFIS
1. MSE	0.86779	0.14528	0.05367
2. RMSE	0.93155	0.38116	0.23166
3. MAPE	0.021830	0.01889	0.00588
4. MRPD (%)	4.658500	0.77500	0.28600
5. HYBRID	0.05448	0.00912	0.00337
6. MPSED	$9.864\ 6 \times 10^{-6}$	2.8552×10^{-8}	1.73532×10^{-8}
7. R	0.96775	0.99372	0.99769
8. R^2	0.93653	0.98748	0.99538
9. adj. R^2	0.93301	0.98679	0.99512

model performance.[53] Therefore, the error analysis revealed the superiority of ANFIS at simulating the oxidation process of benzyl alcohol to benzaldehyde over RSM and ANN techniques. The actual experimental values as well as the predicted values of benzaldehyde yield for the three models were plotted against the run numbers (Figure 9b). It can be seen from the figure that the ANN model was the least accurate, which is corroborated by its very high MRPD of 4.7% (Table 7).

3.6. Proposed Mechanism for the Selective Oxidation of Benzyl Alcohol and Its Greenness. Although the mechanism is still a matter of discussion, Figure 10 illustrates the proposed mechanism. The catalyst having an abundance of oxygen, cerium, and zirconium species $[M^{n+}]$ may activate the TBHP oxidant, which would then selectively oxidize benzyl alcohol to benzaldehyde.[107] The release of the TBHP proton to the solution by protonation was made possible by the coordination of each molecule of TBPH on the catalyst surface. With the proton being picked by the oxygen atom in the alcohol, the *tert*-butyl radicals act like nucleophiles attacking the catalyst. The active site on the catalyst would respond by binding the *tert*-butyl radical and under high concentrations of alcohol, and the majority of the metal site will be coordinated, forming an intermediate "metal alcoholate". A metal hydride shift would occur in this metal alcoholate species, producing a metal-hydride intermediate and the benzaldehyde product.[108,109] Both the hydride shift and the breakdown of the metal alcoholate link will occur asynchronously but in unison. Compared to the breaking of the metal alcoholate bond, the hydride shift would proceed more quickly. The rapid oxidation of the metal hydride by oxygen to produce water while regenerating the original metallic site will be the last stage.

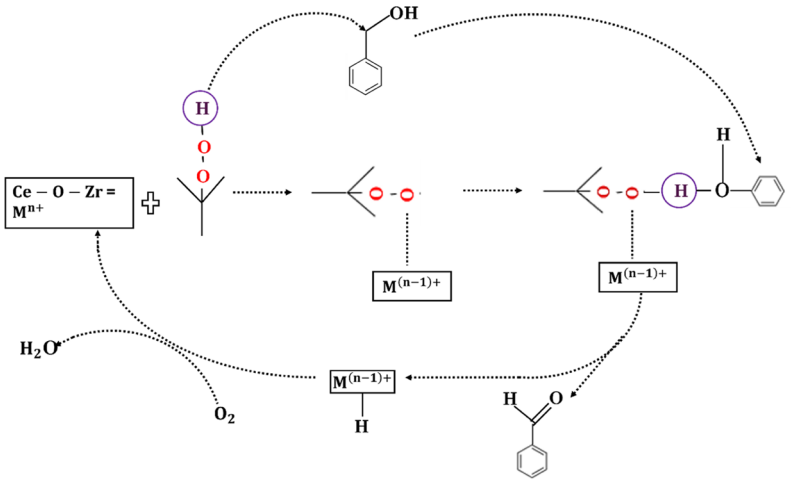

Figure 10. Mechanism of selective oxidation of benzyl alcohol over the $Ce_{0.8}Zr_{0.2}O_2$ catalyst.

https://doi.org/10.1021/acsomega.4c02174
ACS Omega 2024, 9, 34464−34481

Furthermore, a chemical reaction can be gauged green using sustainable green metrics parameters like mass productivity (MP), mass intensity (MI), and environmental factor (*E*-factor). These green parameters were determined for the production of benzaldehyde, and Table S3 in the Supporting Information shows their relevant values. MP, MI, and *E*-factor should all be low in a typical green reaction, indicating that the designed protocol is both extremely cost-effective and environmentally benign.[110] As can be observed, the model reaction produced an *E*-factor of 1.57, an MI-value of 2.57, and an MP-value of 38%, all very desirable results for environmentally friendly and sustainable organic synthesis.

4. REUSABILITY ANALYSIS

In the reusability experiment of benzyl alcohol oxidation with the TBHP oxidant using optimal conditions, the catalyst was recovered after each use, cleaned, and dried in the oven before being recalcined at 450 °C for 12 h to be utilized again in a fresh reaction cycle. Figure 11 displays comparative graphics

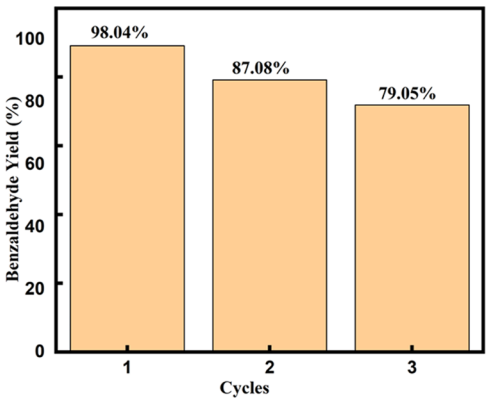

Figure 11. $Ce_{0.8}Zr_{0.2}O_2$ catalysts' reusability at optimum reaction conditions.

that indicate the catalyst reutilization capability for three consecutive tests. It was shown that following the catalyst's three consecutive uses, the benzaldehyde yield stays above 60%, decreasing from 98.04 to 79.05%.[111−113] The reduction in the efficiency of the catalyst reuse can be attributed to either catalyst leaching or the loss of active sites on the catalyst surface.

5. FUTURE PERSPECTIVE AND CONCLUSIONS

This study mainly focused only on experimental investigations and the optimization of the benzyl alcohol oxidation process employing three input factors while keeping the refluxing speed and the quantity of oxidant utilized constant. Future research should consider varying the five components as well as the potential of process optimization and prediction. Although optimal parameters are crucial for industries to scale up, scalability may be limited by factors including reactor design, material cost, scale-up deadlines, etc. Additionally, the literature reveals other investigations that selectively produce benzaldehyde using different oxidants and heterogeneous catalyst types without the application of machine learning. As a result, a great deal of research and development is yet to be done with respect to mathematical modeling and application of optimization tools in benzaldehyde production. Therefore, it will be interesting to continue developing, assessing, and contrasting various models in relation to the optimization and prediction of benzaldehyde yield.

On the other hand, using the inverse micelle method to synthesize mesoporous ceria-zirconium catalyst ($Ce_{0.8}Zr_{0.2}O_2$), and TBHP as the oxygen donor, was successful in evaluating the percentage yield of benzaldehyde from benzyl alcohol oxidation under ideal reaction conditions. The selected oxidation parameters of benzyl alcohol conversion with TBHP were examined and evaluated to determine the maximum percentage yield of benzaldehyde. The prepared mesoporous ceria-zirconium was found to be an efficient, stable, and reusable catalyst for the oxidation of benzyl alcohol. The introduction of zirconium species into the lattice structure of the cerium support resulted in enhanced catalytic activity. The response of the oxidation process with input parameters was designed and optimized using the RSM, ANN, and ANFIS models. For optimal oxidation efficiency, the ideal values of three process parameters were estimated. The three models that were examined were found to be competent in the selective production of benzaldehyde percentage yield. With a higher coefficient of determination value (R^2) of 0.99538, the ANFIS model demonstrated that its predictions outperform that of RSM and the ANN model, which has (R^2) values of 0.98748 and 0.93653. Additional analyses were performed using the RSM and ANFIS 3D-model plots, illustrating the interacting effects with independent variables. A statistical comparison of the models shows that good performance is indicated by lower error values for MSE, MRPD, HYBRID, MPSED, MAPE, RMSE, and MAPE. With the indicated lower MSE values, ANFIS (0.05367) followed by RSM (0.1452) is statistically more reliable in maximizing and forecasting the oxidation parameters of benzyl alcohol using TBHP. The ANFIS model's negligible residual errors demonstrated how closely the experimental data approximated their predicted values. In addition, the green chemistry matrix calculations for the reaction showed lower values of *E*-factor (1.57), MI (2.57), and MP (38%), which are highly desirable for green and sustainable reactions.

■ ASSOCIATED CONTENT

Supporting Information

The Supporting Information is available free of charge at https://pubs.acs.org/doi/10.1021/acsomega.4c02174.

Statistical error equations (eqs S1−S6), experimental design values using the central composite design of RSM (Table S1), experimental and predicted values of yield using RSM, ANN, and ANFIS (Table S2), RSM residual analysis (Figure S1), RSM perturbation plot (Figure S2), Ramp desirability analysis (Figure S3), ANN modeling plots showing the best validation performance for benzyl alcohol oxidation and error histogram (Figure S4), ANFIS modeling plot showing Sugeno-fuzzy architecture for benzyl alcohol oxidation and distribution plot for the trained data set (Figure S5), ANFIS 3D plots and optimization rule viewer plot (Figure S6), and green metrics calculations for benzaldehyde production (Table S3) (PDF)

■ AUTHOR INFORMATION

Corresponding Author

Ikenna Chibuzor Emeji − *Faculty of Science, Department of Chemical Sciences-APK, University of Johannesburg,*

https://doi.org/10.1021/acsomega.4c02174
ACS Omega 2024, 9, 34464−34481

Johannesburg 2006, South Africa; orcid.org/0000-0002-8164-3539; Email: emejiiyk@gmail.com

Authors

Michael Kumi − *CSIR - Water Research Institute, Accra, Ghana*

Reinout Meijboom − *Faculty of Science, Department of Chemical Sciences-APK, University of Johannesburg, Johannesburg 2006, South Africa;* orcid.org/0000-0003-0901-5690

Complete contact information is available at: https://pubs.acs.org/10.1021/acsomega.4c02174

Notes

The authors declare no competing financial interest.

■ ACKNOWLEDGMENTS

The Department of Chemical Sciences (formerly known as Applied Chemistry) at the University of Johannesburg, South Africa, is acknowledged by the authors for offering a suitable environment to conduct this study. A special thanks also goes to the "Metacatalysis research group" especially "Tafadzwa Precious Mabate and Aisha Ayibongwe Khumalo" for their unwavering support throughout this project.

■ NOMENCLATURE

ANN	artificial neural network
RSM	response surface methodology
ANFIS	adaptive neuro-fuzzy inference system
TBHP	*tert*-butyl hydroperoxide
BBD	Box−Behnken experimental design
ORC	oxygen release capacity
OSC	oxygen storage capacity
P-123	(poly(ethylene glycol)-*block*-poly(propylene glycol)-*block*-poly(ethylene glycol))
OFAT	one factor at a time factor
LM	Levenberg−Marquardt
BR	Bayesian regularization
FID	flame ionization detector
CCD	central composite design
ANOVA	analysis of variance
MF	membership functions
F-value	Fisher distribution value
p-values	probability values
df	degree of freedom
XRD	X-ray diffraction
BET	Brunauer−Emmett−Teller
EDX	energy-dispersive X-ray spectroscopy
TEM	transmission electron microscopy
SEM	scanning electron microscopy

■ REFERENCES

(1) Zhang, Y.; Cui, X.; Shi, F.; Deng, Y. Nano-Gold Catalysis in Fine Chemical Synthesis. *Chem. Rev.* **2012**, *112* (4), 2467−2505.

(2) Groppo, E.; Lazzarini, A.; Carosso, M.; Bugaev, A.; Manzoli, M.; Pellegrini, R.; Lamberti, C.; Banerjee, D.; Longo, A. Dynamic Behavior of Pd/P4VP Catalyst during the Aerobic Oxidation of 2-Propanol: A Simultaneous SAXS/XAS/MS Operando Study. *ACS Catal.* **2018**, *8* (8), 6870−6881.

(3) Torbina, V. V.; Vodyankin, A. A.; Ten, S.; Mamontov, G. V.; Salaev, M. A.; Sobolev, V. I.; Vodyankina, O. V. Ag-Based Catalysts in Heterogeneous Selective Oxidation of Alcohols: A Review. *Catalysts* **2018**, *8* (10), 447.

(4) Sankar, M.; He, Q.; Engel, R. V.; Sainna, M. A.; Logsdail, A. J.; Roldan, A.; Willock, D. J.; Agarwal, N.; Kiely, C. J.; Hutchings, G. J. Role of the Support in Gold-Containing Nanoparticles as Heterogeneous Catalysts. *Chem. Rev.* **2020**, *120* (8), 3890−3938.

(5) Xu, S.; Wu, J.; Huang, P.; Lao, C.; Lai, H.; Wang, Y.; Wang, Z.; Zhong, G.; Fu, X.; Peng, F. Selective Catalytic Oxidation of Benzyl Alcohol to Benzaldehyde by Nitrates. *Front Chem.* **2020**, *8*, 151 DOI: 10.3389/fchem.2020.00151.

(6) Pillai, U. Oxidation of Alcohols over Fe3+/Montmorillonite-K10 Using Hydrogen Peroxide. *Appl. Catal., A* **2003**, *245* (1), 103−109.

(7) Lingaiah, N.; Reddy, K. M.; Babu, N. S.; Rao, K. N.; Suryanarayana, I.; Prasad, P. S. S. Aerobic Selective Oxidation of Benzyl Alcohol over Vanadium Substituted Ammonium Salt of 12-Molybdophosphoric Acid. *Catal. Commun.* **2006**, *7* (4), 245−250.

(8) Della Pina, C.; Falletta, E.; Rossi, M. Highly Selective Oxidation of Benzyl Alcohol to Benzaldehyde Catalyzed by Bimetallic Gold−Copper Catalyst. *J. Catal.* **2008**, *260* (2), 384−386.

(9) Choudhary, V. R.; Dumbre, D. K.; Bhargava, S. K. Oxidation of Benzyl Alcohol to Benzaldehyde by *Tert* -Butyl Hydroperoxide over Nanogold Supported on TiO_2 and Other Transition and Rare-Earth Metal Oxides. *Ind. Eng. Chem. Res.* **2009**, *48* (21), 9471−9478.

(10) Crombie, C. M.; Lewis, R. J.; Taylor, R. L.; Morgan, D. J.; Davies, T. E.; Folli, A.; Murphy, D. M.; Edwards, J. K.; Qi, J.; Jiang, H.; Kiely, C. J.; Liu, X.; Skjøth-Rasmussen, M. S.; Hutchings, G. J. Enhanced Selective Oxidation of Benzyl Alcohol via *In Situ* H_2O_2 Production over Supported Pd-Based Catalysts. *ACS Catal.* **2021**, *11* (5), 2701−2714.

(11) Vijayakumar, B.; Chowreddy, R. R.; et al. Synthesis of P-Tolyl Stearate Catalyzed by Acid Activated Indian Bentonite. *Indian J. Chem. Technol.* **2005**, *12* (3), 316−321.

(12) Schultz, M. J.; Sigman, M. S. Recent Advances in Homogeneous Transition Metal-Catalyzed Aerobic Alcohol Oxidations. *Tetrahedron* **2006**, *62* (35), 8227−8241.

(13) Chan-Thaw, C. E.; Savara, A.; Villa, A. Selective Benzyl Alcohol Oxidation over Pd Catalysts. *Catalysts* **2018**, *8* (10), 431.

(14) Xu, C.; Zhang, C.; Li, H.; Zhao, X.; Song, L.; Li, X. An Overview of Selective Oxidation of Alcohols: Catalysts, Oxidants and Reaction Mechanisms. *Catal. Surv. Asia* **2016**, *20* (1), 13−22.

(15) Lukato, S.; Wendt, O. F.; Wallenberg, R.; Kasozi, G. N.; Naziriwo, B.; Persson, A.; Folkers, L. C.; Tebandeke, E. Selective Oxidation of Benzyl Alcohols with Molecular Oxygen as the Oxidant Using Ag-Cu Catalysts Supported on Polyoxometalates. *Results Chem.* **2021**, *3*, No. 100150.

(16) Sheldon, R. A. Organic Synthesis-Past, Present and Future. *Chem. Ind.* **1992**, 903−906.

(17) Sheldon, R. A. Metrics of Green Chemistry and Sustainability: Past, Present, and Future. *ACS Sustainable Chem. Eng.* **2018**, *6* (1), 32−48.

(18) Sheldon, R. A. The E Factor 25 Years on: The Rise of Green Chemistry and Sustainability. *Green Chem.* **2017**, *19* (1), 18−43.

(19) Constable, D. J. C.; Curzons, A. D.; Cunningham, V. L. Metrics to 'Green' Chemistry—Which Are the Best? *Green Chem.* **2002**, *4* (6), 521−527.

(20) Clarke, C. J.; Tu, W.-C.; Levers, O.; Bröhl, A.; Hallett, J. P. Green and Sustainable Solvents in Chemical Processes. *Chem. Rev.* **2018**, *118* (2), 747−800.

(21) Sheldon, R. A.; Bode, M. L.; Akakios, S. G. Metrics of Green Chemistry: Waste Minimization. *Curr. Opin. Green Sustainable Chem.* **2022**, *33*, No. 100569.

(22) Dicks, A. P.; Hent, A. The E Factor and Process Mass Intensity. In *Springer Briefs in Molecular Science*, Green Chemistry Metrics; Springer International Publishing, 2015; pp 45−67 DOI: 10.1007/978-3-319-10500-0_3.

(23) Curzons, A. D.; Mortimer, D. N.; Constable, D. J. C.; Cunningham, V. L. So You Think Your Process Is Green, How Do You Know? — Using Principles of Sustainability to Determine What Is Green − a Corporate Perspective. *Green Chem.* **2001**, *3* (1), 1−6.

(24) Pudukudy, M.; Yaakob, Z.; Narayanan, B. Selective Vapour Phase Oxidation of Benzyl Alcohol to Benzaldehyde over Mesoporous

Ceria−Zirconia Solid Solution Synthesized Via a Facile Citrate Route. *J. Clust Sci.* **2014**, *25* (6), 1599−1614.
(25) Dossumov, K.; Ergazieva, G. E.; Ermagambet, B. T.; Telbayeva, M. M.; Mambetova, M. M.; Myltykbayeva, L. K.; Kassenova, Z. M. Role of Ceria in Several Energy-Related Catalytic Transformations. *Chem. Pap.* **2020**, *74* (2), 373−388.
(26) Olivan, A. M.; Kremenic, G.; Fierro, J. L. G. Dehydration-Dehydrogenation of 1- and 2-Butanols on Lanthanide Oxide Catalysts. *React. Kinet. Catal. Lett.* **1985**, *27* (1), 53−57.
(27) Jin, H.; Chen, J.; Mao, S.; Wang, Y. Transition Metal Induced the Contraction of Tungsten Carbide Lattice as Superior Hydrogen Evolution Reaction Catalyst. *ACS Appl. Mater. Interfaces* **2018**, *10* (26), 22094−22101.
(28) Boettcher, S. W.; Fan, J.; Tsung, C.-K.; Shi, Q.; Stucky, G. D. Harnessing the Sol−Gel Process for the Assembly of Non-Silicate Mesostructured Oxide Materials. *Acc. Chem. Res.* **2007**, *40* (9), 784−792.
(29) Schüth, F. Non-Siliceous Mesostructured and Mesoporous Materials. *Chem. Mater.* **2001**, *13* (10), 3184−3195.
(30) Deng, J.; Zhou, Y.; Cui, Y.; Lan, L.; Wang, J.; Yuan, S.; Chen, Y. The Influence of H2O2 on the Properties of CeO2-ZrO2Mixed Oxides. *J. Mater. Sci.* **2017**, *52* (9), 5242−5255.
(31) Allan, M.; Grinter, D.; Dhaliwal, S.; Muryn, C.; Forrest, T.; Maccherozzi, F.; Dhesi, S. S.; Thornton, G. Redox Behaviour of a Ceria−Zirconia Inverse Model Catalyst. *Surf. Sci.* **2019**, *682*, 8−13.
(32) Poyraz, A. S.; Kuo, C.-H.; Biswas, S.; King'ondu, C. K.; Suib, S. L. A General Approach to Crystalline and Monomodal Pore Size Mesoporous Materials. *Nat. Commun.* **2013**, *4* (1), No. 2952.
(33) Pérez, Y.; Ballesteros, R.; Fajardo, M.; Sierra, I.; del Hierro, I. Copper-Containing Catalysts for Solvent-Free Selective Oxidation of Benzyl Alcohol. *J. Mol. Catal. A: Chem.* **2012**, *352*, 45−56.
(34) Ali, J. K. Neural Networks: A New Tool for the Petroleum Industry? In *All Days*; SPE, 1994 DOI: 10.2118/27561-MS.
(35) Rekhate, C. V.; Shrivastava, J. K. Decolorization of Azo Dye Solution by Ozone Based Advanced Oxidation Processes: Optimization Using Response Surface Methodology and Neural Network. *Ozone Sci. Eng.* **2020**, *42* (6), 492−506.
(36) Onu, C. E.; Igbokwe, P. K.; Nwabanne, J. T.; Ohale, P. E. ANFIS, ANN, and RSM Modeling of Moisture Content Reduction of Cocoyam Slices. *J. Food Process Preserv.* **2022**, *46* (1), No. e16032, DOI: 10.1111/jfpp.16032.
(37) Jazayeri, K.; Jazayeri, M.; Uysal, S. Comparative Analysis of Levenberg-Marquardt and Bayesian Regularization Backpropagation Algorithms in Photovoltaic Power Estimation Using Artificial Neural Network. In *Advances in Data Mining. Applications and Theoretical Aspects*, Lecture Notes in Computer Science; Springer International Publishing, 2016; pp 80−95. DOI: 10.1007/978-3-319-41561-1_7.
(38) Fan, M.; Li, T.; Hu, J.; Cao, R.; Wei, X.; Shi, X.; Ruan, W. Artificial Neural Network Modeling and Genetic Algorithm Optimization for Cadmium Removal from Aqueous Solutions by Reduced Graphene Oxide-Supported Nanoscale Zero-Valent Iron (NZVI/RGO) Composites. *Materials* **2017**, *10* (5), 544.
(39) Aydın Temel, F.; Cagcag Yolcu, O.; Turan, N. G. Artificial Intelligence and Machine Learning Approaches in Composting Process: A Review. *Bioresour. Technol.* **2023**, *370*, No. 128539.
(40) Mogudi, B. M.; Ncube, P.; Meijboom, R. Catalytic Activity of Mesoporous Cobalt Oxides with Controlled Porosity and Crystallite Sizes: Evaluation Using the Reduction of 4-Nitrophenol. *Appl. Catal., B* **2016**, *198*, 74−82.
(41) Fukuda, I. M.; Pinto, C. F. F.; Moreira, C. d. S.; Saviano, A. M.; Lourenço, F. R. Design of Experiments (DoE) Applied to Pharmaceutical and Analytical Quality by Design (QbD). *Braz. J. Pharm. Sci.* **2018**, *54* (spe). DOI: 10.1590/s2175-97902018000001006.
(42) Khuri, A. I.; Mukhopadhyay, S. Response Surface Methodology. *Wiley Interdiscip. Rev.: Comput. Stat.* **2010**, *2* (2), 128−149.
(43) Ositadinma, I. C.; Tagbo, N. J.; Elijah, O. C. Optimum Process Parameters for Activated Carbon Production from Rice Husk for Phenol Adsorption. *Curr. J. Appl. Sci. Technol.* **2019**, 1−11.
(44) Venkatesh Prabhu, M.; Karthikeyan, R. Comparative Studies on Modelling and Optimization of Hydrodynamic Parameters on Inverse Fluidized Bed Reactor Using ANN-GA and RSM. *Alexandria Eng. J.* **2018**, *57* (4), 3019−3032.
(45) de Oliveira, L. G.; de Paiva, A. P.; Balestrassi, P. P.; Ferreira, J. R.; da Costa, S. C.; da Silva Campos, P. H. Response Surface Methodology for Advanced Manufacturing Technology Optimization: Theoretical Fundamentals, Practical Guidelines, and Survey Literature Review. *Int. J. Adv. Manuf. Technol.* **2019**, *104* (5−8), 1785−1837.
(46) Myers, R. H. *Response Surface Methodology: Process and Product Optimization Using Designed Experiments*; John Wiley & Sons, 2016.
(47) Tong, L.-I.; Chang, Y.-C.; Lin, S.-H. Determining the Optimal Re-Sampling Strategy for a Classification Model with Imbalanced Data Using Design of Experiments and Response Surface Methodologies. *Expert Syst. Appl.* **2011**, *38* (4), 4222−4227.
(48) Mugendiran, V.; Gnanavelbabu, A.; Ramadoss, R. Parameter Optimization for Surface Roughness and Wall Thickness on AA5052 Aluminium Alloy by Incremental Forming Using Response Surface Methodology. *Procedia Eng.* **2014**, *97*, 1991−2000.
(49) Kumari, S.; Verma, A.; Sharma, P.; Agarwal, S.; Rajput, V. D.; Minkina, T.; Rajput, P.; Singh, S. P.; Garg, M. C. Introducing Machine Learning Model to Response Surface Methodology for Biosorption of Methylene Blue Dye Using Triticum Aestivum Biomass. *Sci. Rep.* **2023**, *13* (1), No. 8574.
(50) Wang, W.; Cheng, Y.; Tan, G. Design Optimization of SBS-Modified Asphalt Mixture Reinforced with Eco-Friendly Basalt Fiber Based on Response Surface Methodology. *Materials* **2018**, *11* (8), 1311.
(51) Thakkar, K.; Kachhawaha, S. S.; Kodgire, P.; Keshav, M. Effectiveness of RSM Based Central Composite Design for Optimization of In-Situ Biodiesel Production Process from Castor Seeds. *IOP Conf. Ser.: Mater. Sci. Eng.* **2021**, *1146* (1), No. 012008.
(52) Kumari, S.; Rajput, V. D.; Minkina, T.; Rajput, P.; Sharma, P.; Verma, A. K.; Agarwal, S.; Garg, M. C. Application of RSM for Bioremoval of Methylene Blue Dye from Industrial Wastewater onto Sustainable Walnut Shell (Juglans Regia) Biomass. *Water* **2022**, *14* (22), 3651.
(53) Aigbe, U. O.; Lebepe, T. C.; Oluwafemi, O. S.; Osibote, O. A. Prediction and Optimizing of Methylene Blue Sequestration to Activated Charcoal/Magnetic Nanocomposites Using Artificial Neutral Network and Response Surface Methodology. *Chemosphere* **2024**, *355*, No. 141751.
(54) Aghilesh, K.; Kumar, A.; Agarwal, S.; Garg, M. C.; Joshi, H. Use of Artificial Intelligence for Optimizing Biosorption of Textile Wastewater Using Agricultural Waste. *Environ. Technol.* **2023**, *44* (1), 22−34.
(55) Khodadoust, S.; Sadeghi, H.; Pebdani, A. A.; Mohammadi, J.; Salehi, A. Optimization of Ultrasound-Assisted Extraction of Colchicine Compound from Colchicum Haussknechtii by Using Response Surface Methodology. *J. Saudi Soc. Agric. Sci.* **2017**, *16* (2), 163−170.
(56) Sahu, P. K.; Ramisetti, N. R.; Cecchi, T.; Swain, S.; Patro, C. S.; Panda, J. An Overview of Experimental Designs in HPLC Method Development and Validation. *J. Pharm. Biomed. Anal.* **2018**, *147*, 590−611.
(57) Singh, K. P.; Gupta, S.; Singh, A. K.; Sinha, S. Experimental Design and Response Surface Modeling for Optimization of Rhodamine B Removal from Water by Magnetic Nanocomposite. *Chem. Eng. J.* **2010**, *165* (1), 151−160.
(58) Betiku, E.; Osunleke, A. S.; Odude, V. O.; Bamimore, A.; Oladipo, B.; Okeleye, A. A.; Ishola, N. B. Performance Evaluation of Adaptive Neuro-Fuzzy Inference System, Artificial Neural Network and Response Surface Methodology in Modeling Biodiesel Synthesis from Palm Kernel Oil by Transesterification. *Biofuels* **2021**, *12* (3), 339−354.
(59) Pilkington, J. L.; Preston, C.; Gomes, R. L. Comparison of Response Surface Methodology (RSM) and Artificial Neural Networks (ANN) towards Efficient Extraction of Artemisinin from Artemisia Annua. *Ind. Crops Prod.* **2014**, *58*, 15−24.

https://doi.org/10.1021/acsomega.4c02174
ACS Omega 2024, 9, 34464−34481

(60) Poh, P. E.; Gouwanda, D.; Mohan, Y.; Gopalai, A. A.; Tan, H. M. Optimization of Wastewater Anaerobic Digestion Using Mechanistic and Meta-Heuristic Methods: Current Limitations and Future Opportunities. *Water Conserv. Sci. Eng.* **2016**, *1* (1), 1−20.
(61) Ansari, H. R.; Zarei, M. J.; Sabbaghi, S.; Keshavarz, P. A New Comprehensive Model for Relative Viscosity of Various Nanofluids Using Feed-Forward Back-Propagation MLP Neural Networks. *Int. Commun. Heat Mass Transfer* **2018**, *91*, 158−164.
(62) Bezerra, M. A.; Santelli, R. E.; Oliveira, E. P.; Villar, L. S.; Escaleira, L. A. Response Surface Methodology (RSM) as a Tool for Optimization in Analytical Chemistry. *Talanta* **2008**, *76* (5), 965−977.
(63) Onu, C. E.; Igbokwe, P. K.; Nwabanne, J. T.; Nwajinka, C. O.; Ohale, P. E. Evaluation of Optimization Techniques in Predicting Optimum Moisture Content Reduction in Drying Potato Slices. *Artif. Intell. Agric.* **2020**, *4*, 39−47.
(64) Barahona, J.; Sun, H.-M. A Process for Exploring Employees' Relationships via Social Network and Sentiment Analysis. In *Data Mining and Big Data*, Lecture Notes in Computer Science; Springer International Publishing, 2017; pp 3−8 DOI: 10.1007/978-3-319-61845-6_1.
(65) Khoshnevisan, B.; Rafiee, S.; Omid, M.; Mousazadeh, H. Development of an Intelligent System Based on ANFIS for Predicting Wheat Grain Yield on the Basis of Energy Inputs. *Inf. Process. Agric.* **2014**, *1* (1), 14−22.
(66) Mashaly, A. F.; Alazba, A. Assessing the Accuracy of ANN, ANFIS, and MR Techniques in Forecasting Productivity of an Inclined Passive Solar Still in a Hot, Arid Environment. *Water SA* **2019**, *45* (2 April), 239−250, DOI: 10.4314/wsa.v45i2.11.
(67) Rosadi, D. Analysis of Financial Time Series Data Using Adaptive Neuro Fuzzy Inference System (ANFIS). *Int. J. Comput. Sci. Issues (IJCSI)* **2013**, *10* (2), 491−496.
(68) Babanezhad, M.; Nakhjiri, A. T.; Shirazian, S. Changes in the Number of Membership Functions for Predicting the Gas Volume Fraction in Two-Phase Flow Using Grid Partition Clustering of the ANFIS Method. *ACS Omega* **2020**, *5* (26), 16284−16291.
(69) Gonzalez del Cerro, R. T.; Subathra, M. S. P.; Manoj Kumar, N.; Verrastro, S.; Thomas George, S. Modelling the Daily Reference Evapotranspiration in Semi-Arid Region of South India: A Case Study Comparing ANFIS and Empirical Models. *Inf. Process. Agric.* **2021**, *8* (1), 173−184.
(70) Kiran, T. R.; Rajput, S. P. S. An Effectiveness Model for an Indirect Evaporative Cooling (IEC) System: Comparison of Artificial Neural Networks (ANN), Adaptive Neuro-Fuzzy Inference System (ANFIS) and Fuzzy Inference System (FIS) Approach. *Appl. Soft Comput.* **2011**, *11* (4), 3525−3533.
(71) Dodo, U. A.; Ashigwuike, E. C.; Emechebe, J. N.; Abba, S. I. Prediction of Energy Content of Biomass Based on Hybrid Machine Learning Ensemble Algorithm. *Energy Nexus* **2022**, *8*, No. 100157.
(72) Trovarelli, A.; Zamar, F.; Llorca, J.; de Leitenburg, C.; Dolcetti, G.; Kiss, J. T. Nanophase Fluorite-Structured CeO2−ZrO2Catalysts Prepared by High-Energy Mechanical Milling. *J. Catal.* **1997**, *169* (2), 490−502.
(73) Faqeeh, A. J.; Ali, T. T.; Basahel, S. N.; Narasimharao, K. Nanosized Samarium Modified Au-Ce 0.5 Zr 0.5 O 2 Catalysts for Oxidation of Benzyl Alcohol. *Molecular Catalysis* **2018**, *456*, 10−21.
(74) Matharu, A. S.; Ahmed, S.; Almonthery, B.; Macquarrie, D. J.; Lee, Y.; Kim, Y. Starbon/High-Amylose Corn Starch-Supported N-Heterocyclic Carbene−Iron(III) Catalyst for Conversion of Fructose into 5-Hydroxymethylfurfural. *ChemSusChem* **2018**, *11* (4), 716−725.
(75) Suresh, R.; Ponnuswamy, V.; Mariappan, R. Effect of Annealing Temperature on the Microstructural, Optical and Electrical Properties of CeO2 Nanoparticles by Chemical Precipitation Method. *Appl. Surf. Sci.* **2013**, *273*, 457−464.
(76) Nusrath, K.; Muraleedharan, K. Synthesis, Characterization and Thermal Decomposition Kinetics of Cerium Oxalate Rods. *Devagiri J. Sci.* **2016**, *2* (1), 118−120.
(77) Thommes, M.; Kaneko, K.; Neimark, A. V.; Olivier, J. P.; Rodriguez-Reinoso, F.; Rouquerol, J.; Sing, K. S. W. Physisorption of Gases, with Special Reference to the Evaluation of Surface Area and Pore Size Distribution (IUPAC Technical Report). *Pure Appl. Chem.* **2015**, *87* (9−10), 1051−1069.
(78) Yang, Z.; Qin, G.; Tang, R.; Jia, L.; Wang, F.; Liu, T. Formaldehyde Oxidation of Ce0.8Zr0.2O2 Nanocatalysts for Room Temperature: Kinetics and Effect of PH Value. *Nanomaterials* **2023**, *13* (14), 2074.
(79) Cao, J.-L.; Deng, Q.-F.; Yuan, Z.-Y. Mesoporous Ce0.8Zr0.2O2 Solid Solutions-Supported CuO Nanocatalysts for CO Oxidation: A Comparative Study of Preparation Methods. *J. Mater. Sci.* **2009**, *44* (24), 6663−6669.
(80) Guo, X.; Hu, D.; Li, Y.; Duan, J.; Zhang, X.; Fan, X.; Duan, H.; Li, W. Theoretical Progress and Key Technologies of Onshore Ultra-Deep Oil/Gas Exploration. *Engineering* **2019**, *5* (3), 458−470.
(81) Wang, Z.-j.; Xie, Y.; Liu, C. Synthesis and Characterization of Noble Metal (Pd, Pt, Au, Ag) Nanostructured Materials Confined in the Channels of Mesoporous SBA-15. *J. Phys. Chem. C* **2008**, *112* (50), 19818−19824.
(82) Cushing, B. L.; Kolesnichenko, V. L.; O'Connor, C. J. Recent Advances in the Liquid-Phase Syntheses of Inorganic Nanoparticles. *Chem. Rev.* **2004**, *104* (9), 3893−3946.
(83) Hadi, A.; Nazri Abu Shah, M.; Ismail, K. N.; Ismail, R. Novel Synthesis of High Surface Area Nano-$CeZrO_2$: Transformation of the Microstructure and Textural Properties as the Effect of Calcination. *Adv. Nat. Sci.: Nanosci. Nanotechnol.* **2018**, *9* (4), No. 045015.
(84) Long, W.; Chen, Z.; Huang, Y.; Kang, X. Selective Oxidation of Toluene to Benzaldehyde Using Co-ZIF Nano-Catalyst. *Int. J. Mol. Sci.* **2022**, *23* (21), 12881.
(85) Ndolomingo, M. J.; Meijboom, R. Selective Liquid Phase Oxidation of Benzyl Alcohol to Benzaldehyde by Tert-Butyl Hydroperoxide over γ-Al2O3 Supported Copper and Gold Nanoparticles. *Appl. Surf. Sci.* **2017**, *398*, 19−32.
(86) Choudhary, V. R.; Dumbre, D. K.; Narkhede, V. S.; Jana, S. K. Solvent-Free Selective Oxidation of Benzyl Alcohol and Benzaldehyde by Tert-Butyl Hydroperoxide Using MnO- 4-Exchanged Mg−Al−Hydrotalcite Catalysts. *Catal. Lett.* **2003**, *86* (4), 229−233.
(87) Darakhshan, S.; Fatehi, A.; Hassanshahi, G.; Mahmoodi, S.; Hashemi, M. S.; Karimabad, M. N. Serum Concentration of Angiogenic (CXCL1, CXCL12) and Angiostasis (CXCL9, CXCL10) CXC Chemokines Are Differentially Altered in Normal and Gestational Diabetes Mellitus Associated Pregnancies. *J. Diabetes Metab. Disord.* **2019**, *18* (2), 371−378.
(88) Popp, P. F.; Benjdia, A.; Strahl, H.; Berteau, O.; Mascher, T. The Epipeptide YydF Intrinsically Triggers the Cell Envelope Stress Response of Bacillus Subtilis and Causes Severe Membrane Perturbations. *Front. Microbiol.* **2020**, *11*, 151 DOI: 10.3389/fmicb.2020.00151.
(89) Ahmadi, S.; Khormali, A.; Meerovich Khoutoriansky, F. Optimization of the Demulsification of Water-in-Heavy Crude Oil Emulsions Using Response Surface Methodology. *Fuel* **2022**, *323*, No. 124270.
(90) Nair, A. T.; Makwana, A. R.; Ahammed, M. M. The Use of Response Surface Methodology for Modelling and Analysis of Water and Wastewater Treatment Processes: A Review. *Water Sci. Technol.* **2014**, *69* (3), 464−478.
(91) Zhao, X.; Baharinikoo, L.; Farahani, M.; et al. Experimental Modelling Studies on the Removal of Dyes and Heavy Metal Ions Using ZnFe2O4 Nanoparticle. *Sci. Rep.* **2022**, *12* (1), No. 5987.
(92) Rahbar, R. S.; Haji, A. Use of D-optimal Design to Model and the Analysis of the Effect of the Draw Ratio on Some Physical Properties of Hot Multistage Drawn Nylon 6 Fibers. *J. Appl. Polym. Sci.* **2013**, *130* (2), 1337−1344.
(93) Collins, O. N.; Elijah, O. C. ADSORPTION OF A DYE (CRYSTAL VIOLET) ON AN ACID MODIFIED NON-CONVENTIONAL ADSORBENT. *J. Chem. Technol. Metall.* **2019**, *54* (1), 95−110.
(94) Alizadeh, M.; Sadrameli, S. M. Numerical Modeling and Optimization of Thermal Comfort in Building: Central Composite Design and CFD Simulation. *Energy Build* **2018**, *164*, 187−202.

https://doi.org/10.1021/acsomega.4c02174
ACS Omega 2024, 9, 34464−34481

(95) Hamze, H.; Akia, M.; Yazdani, F. Optimization of Biodiesel Production from the Waste Cooking Oil Using Response Surface Methodology. *Process Saf. Environ. Prot.* **2015**, *94*, 1−10.
(96) Bhaumik, M.; Setshedi, K.; Maity, A.; Onyango, M. S. Chromium(VI) Removal from Water Using Fixed Bed Column of Polypyrrole/Fe3O4 Nanocomposite. *Sep. Purif. Technol.* **2013**, *110*, 11−19.
(97) Zenebe, A.; Kabir-ud-Din; Mohammed Yimer, A.; Kuzhunellil, S.; Demissie, H. Green Synthesis of Magnetic Nanocomposite by Leave Extract for the Treatment of Methylene Blue Contaminated Water. *Chem. Eng. J. Adv.* **2021**, *8*, No. 100193.
(98) Rosly, N. Z.; Abdullah, A. H.; Ahmad Kamarudin, M.; Ashari, S. E.; Alang Ahmad, S. A. Adsorption of Methylene Blue Dye by Calix[6]Arene-Modified Lead Sulphide (Pbs): Optimisation Using Response Surface Methodology. *Int. J. Environ. Res. Public Health* **2021**, *18* (2), 397.
(99) Wu, J.; Wang, J.-L.; Li, M.-H.; Lin, J.-P.; Wei, D.-Z. Optimization of Immobilization for Selective Oxidation of Benzyl Alcohol by Gluconobacter Oxydans Using Response Surface Methodology. *Bioresour. Technol.* **2010**, *101* (23), 8936−8941.
(100) Hatambeygi, N.; Abedi, G.; Talebi, M. Method Development and Validation for Optimised Separation of Salicylic, Acetyl Salicylic and Ascorbic Acid in Pharmaceutical Formulations by Hydrophilic Interaction Chromatography and Response Surface Methodology. *J. Chromatogr. A* **2011**, *1218* (35), 5995−6003.
(101) Yadav, A. K.; Malik, H.; Chandel, S. S. Selection of Most Relevant Input Parameters Using WEKA for Artificial Neural Network Based Solar Radiation Prediction Models. *Renewable Sustainable Energy Rev.* **2014**, *31*, 509−519.
(102) Khademi, F.; Jamal, S. M.; Deshpande, N.; Londhe, S. Predicting Strength of Recycled Aggregate Concrete Using Artificial Neural Network, Adaptive Neuro-Fuzzy Inference System and Multiple Linear Regression. *Int. J. Sustainable Built Environ.* **2016**, *5* (2), 355−369.
(103) Joglekar, A. M.; May, A. T. Product Excellence through Design of Experiments. *Cereal Foods World* **1987**, *32* (12), 857.
(104) Mazaheri, H.; Ghaedi, M.; Ahmadi Azqhandi, M. H.; Asfaram, A. Application of Machine/Statistical Learning, Artificial Intelligence and Statistical Experimental Design for the Modeling and Optimization of Methylene Blue and Cd(II) Removal from a Binary Aqueous Solution by Natural Walnut Carbon. *Phys. Chem. Chem. Phys.* **2017**, *19* (18), 11299−11317.
(105) Ogedjo, M.; Kapoor, A.; Senthil Kumar, P.; Rangasamy, G.; Ponnuchamy, M.; Rajagopal, M.; Nath Banerjee, P. Modeling of Sugarcane Bagasse Conversion to Levulinic Acid Using Response Surface Methodology (RSM), Artificial Neural Networks (ANN), and Fuzzy Inference System (FIS): A Comparative Evaluation. *Fuel* **2022**, *329*, No. 125409.
(106) Olatunji, K. O.; Ahmed, N. A.; Madyira, D. M.; Adebayo, A. O.; Ogunkunle, O.; Adeleke, O. Performance Evaluation of ANFIS and RSM Modeling in Predicting Biogas and Methane Yields from Arachis Hypogea Shells Pretreated with Size Reduction. *Renewable Energy* **2022**, *189*, 288−303.
(107) Choudhary, V. R.; Dumbre, D. K.; Uphade, B. S.; Narkhede, V. S. Solvent-Free Oxidation of Benzyl Alcohol to Benzaldehyde by Tert-Butyl Hydroperoxide Using Transition Metal Containing Layered Double Hydroxides and/or Mixed Hydroxides. *J. Mol. Catal. A: Chem.* **2004**, *215* (1−2), 129−135.
(108) Saunders, M.; Kates, M. R. Rates of Degenerate 1,2-Hydride and 1,2-Methide Shifts from the Carbon-13 Nuclear Magnetic Resonance Spectra of Tertiary Alkyl Cations. *J. Am. Chem. Soc.* **1978**, *100* (22), 7082−7083.
(109) Baráth, E. Hydrogen Transfer Reactions of Carbonyls, Alkynes, and Alkenes with Noble Metals in the Presence of Alcohols/Ethers and Amines as Hydrogen Donors. *Catalysts* **2018**, *8* (12), 671.
(110) Choudhary, P.; Singh Chauhan, S.; Sharma, D.; Kumar, S.; Krishnan, V. Nanoarchitectonics of Sulfonated Boron Nitride for Catalytic Synthesis of Aromatic Nitriles under Mild Conditions. *Chem. Eng. J.* **2023**, *475*, No. 146055.
(111) Mallesham, B.; Sudarsanam, P.; Raju, G.; Reddy, B. M. Design of Highly Efficient Mo and W-Promoted SnO_2 Solid Acids for Heterogeneous Catalysis: Acetalization of Bio-Glycerol. *Green Chem.* **2013**, *15* (2), 478−489.
(112) Hayati, F.; Moradi, S.; Farshineh Saei, S.; Madani, Z.; Giannakis, S.; Isari, A. A.; Kakavandi, B. A Novel, Z-Scheme ZnO@AC@FeO Photocatalyst, Suitable for the Intensification of Photo-Mediated Peroxymonosulfate Activation: Performance, Reactivity and Bisphenol A Degradation Pathways. *J. Environ. Manage* **2022**, *321*, No. 115851.
(113) Kaveh, M.; Rasooli Sharabiani, V.; Amiri Chayjan, R.; Taghinezhad, E.; Abbaspour-Gilandeh, Y.; Golpour, I. ANFIS and ANNs Model for Prediction of Moisture Diffusivity and Specific Energy Consumption Potato, Garlic and Cantaloupe Drying under Convective Hot Air Dryer. *Inf. Process. Agric.* **2018**, *5* (3), 372−387.

https://doi.org/10.1021/acsomega.4c02174
ACS Omega 2024, 9, 34464−34481